Computational and Experimental studies and biological activity prediction on Octrizole- an insight into antidiabetic activity.

Dona Benny[1, a], A. Anuradha[2], Johanan Christian Prasana [3, a]*

[1,3] *Department of Physics, Madras Christian College, East Tambaram, Chennai, 600059, Tamil Nadu, India,*

[a]*university Of Madras, Chennai 600005, Tamilnadu, India*

[2]*PG and Research Department of Physics, Queen Mary's College(A), Chennai-600 004, India*

**Corresponding author: reachjcp@gmail.com*

Abstract

Octrizole, a heterocyclic aromatic compound, was computationally investigated in this work, and computational techniques were chosen considering their efficiency and low cost. Density Functional Theory approach with the basis set B3LYP was employed. A minimum energy structure is obtained. Structure interpretation of the chosen compound was carried out using molecular geometry, Vibrational analysis (theoretical and experimental), and NMR analysis. Stability and reactivity prediction of Octrizole were done using UV analysis and FMO studies. Global parameters provided insights into the electronic properties as well. MEP map presents the reactive sites and possible interactions. NLO properties of the chosen compound were calculated. Topological studies (ELF and LOL) are also done. Molecular interactions were identified in the RDG plot, and atomic charges present in the title compound were studied. Pharmacological studies were carried out to study the drug-like properties, which were also compared with the standard drug Metformin. Ramachandran plot of proteins identifies the protein stability. Molecular docking studies on Octrizole were employed to study the protein-ligand interactions, and the title compound exhibits a better interaction than the standard drug. Theoretical findings predict that Octrizole might be a potential compound to treat Diabetics.

Keywords: DFT, Benzotriazole Moiety, Heterocyclic, Molecular Docking, Anti-Diabetic;

1 Introduction

Benzotriazole derivatives have versatile biological properties and are under wide investigation, where benzotriazole is a bicyclic, heterocyclic compound with two benzene rings and three nitrogen atoms, demonstrating a range of biological and pharmacological characteristics [1, 2]. Benzotriazole derivatives possess antibacterial [3], antiprotozoal [4], antiviral [5], and antiproliferative [6] activity. Most potent antibacterial drugs are heterocyclic molecules with nitrogen atoms. 3-(benzotriazol-1-yl) -1- (4-bromophenyl)-2- (1,2,4-triazol-1-yl) propan-1-one shows great antibacterial activity [7]. Hepatitis C virus and West Nile virus are inhibited by tetra-bromobenzotriazole and its derivatives [8]. The cellular proliferation of several liquid and solid human cancers was inhibited by compounds 3-Aryl-2-(1H-Benzotriazol-1-yl) Acrylo Nitriles [9]. Significant anti-inflammatory and antinociceptive effects were exhibited by 2-(Benzotriazol-1/2-yl) Propionicacids [10]. In the process of finding and developing new drugs, Benzotriazole nucleus seems to be a particularly intriguing scaffold.

Diabetes is an elevated blood glucose level and is a metabolic condition. The search for an ideal anti diabetic drug lowering blood glucose level continues, and its development is still challenging. DFT studies are performed to determine the quantum chemical descriptors that help in drug development. Pharmacokinetic properties, namely, absorption, distribution, metabolism, and excretion (ADME), are essential during drug design in finding potential compounds for diabetes. α-Amylase, an enzyme crucial for breaking down dietary starch into glucose, where large starch molecules cannot cross the blood-brain barrier to supply glucose to the brain. To address this, α-amylase breaks down these large molecules into smaller sugar fragments that can pass through the barrier. Excessive breakdown of starch into sugars leads to elevated blood glucose. In response, insulin triggers cells to absorb and metabolize this surplus sugar, storing it as glycogen for later energy use. In a healthy individual, this cycle of starch breakdown and glucose regulation occurs continuously. However, in certain situations, excessive amylase activity coupled with insufficient insulin or insulin resistance causes blood glucose levels to rise [11]. α-Amylase is crucially targeted in the development of drugs to combat diabetes, and molecular docking studies analyze the interaction of α-Amylase with ligands [12]. Metformin is a standard drug in treating diabetes, and the newly developing drug candidates are being compared with it to study the potential of developing drugs [13].

Potential of benzotriazole derivatives results in choosing the title compound, Octrizole, which has an antidiabetic property. The IUPAC name of chosen compound is 2-(2-Hydroxy-5-tert-

octylphenyl) benzotriazole with molecular formula $C_{20}H_{25}N_3O$, and it contains 49 atoms in total. Chosen compound has a molecular weight of 323.43g/mol. An extensive literature survey reveals that no studies using Density Functional Theory or molecular docking have been carried out as of yet on this compound. In understanding the scope and application of this derivative, an attempt is made to analyze this compound completely. Structural analysis of Octrizole was employed using DFT studies. Biological evaluation was employed to study biological activities and pharmaceutical applications of the title compound.

2 Experimental details

2-(2-Hydroxy-5-tert-octylphenyl) Benzotriazole (98% purity) is sourced from TCI Chemicals, India. FT-IR, FT Raman were employed at SAIF, IITM, India. KBr sampling technique is used for obtaining FT-IR spectrum within a range from 4000 to 400 cm-1, and FT-Raman spectrum is from 4000 to 100 cm-1. Evaluation of Octrizole for *in vitro* cytotoxicity activity on Rat Skeletal Muscle (L6) cell line was held at Radiant Research Services Private Limited, Bangaluru, India.

3 Computational details

Gaussian16W [14] and Gaussview [15] software serve as the tools for DFT calculations. GaussView is used in visualizing optimized structure. Basis set for Gaussian calculations is 6-311 G++ (d,p), and the functional is B3LYP. Vibrational assignments can be acquired using VEDA software [16]. Employing Multiwfn 3.8 [17], wave-functional analysis (ELF, LOL, RDG, and charge transfer) has been performed. Drug-likeness characteristics are assessed using the online SwissADME program [18]. To determine the bioactivity of Octrizole, the PASS online tool [19] is utilized. Molecular docking uses the AutoDock Tools 1.5.6 software [20] and Discovery Studio [21] is utilized for visualization.

3 RESULTS AND DISCUSSION

3.1 Molecular structure

Molecular geometry is the three-dimensional, spatial arrangement of atoms in a molecule. Optimized structure (highly stable and low-energy) for Octrizole was obtained and is given in Fig.1. Bond parameters are presented in Table 1. Longest bonds are seen between carbon atoms due to their repulsive forces. C5–C7 has a maximum bond length of 1.572 Å. Shortest Bond length (0.972Å) was found between O1 and H45, which may be due to the higher electronegativity value of oxygen than hydrogen, and it might be a suitable site for protein

interaction for biological applications. Largest bond angle identified is 129.7◦ and is between N3-C19-C21 and N4-C20-C22. Least bond angle (102.5° °) was identified between N2-N4-C20 atoms and N2-N3-C19 atoms. In the triazole ring, nitrogen atoms (N2-N3, N2-N4) are 1.340 Å apart. Two rings are attached to the triazole group. In ring 1, bond length of C8-C15, C8-C14 is 1.370 Å and C14-C16, C16-C18, C17-C18, C15-C17 is 1.395 Å. The bond length of C19-C20, C20-C22, C22-C24, C21-C23, C19-C21 is 1.407 Å and C23-C24 is 1.421 Å in ring 2. C-H bonds in rings are found to be 1.08 Å apart. Carbon-carbon and carbon-hydrogen bond lengths and bond angles in the rings are responsible for their symmetrical structure [22,23]. The spectrum of values for bond length and bond angle (Table 1) may suggest that the chosen compound might be biologically active.

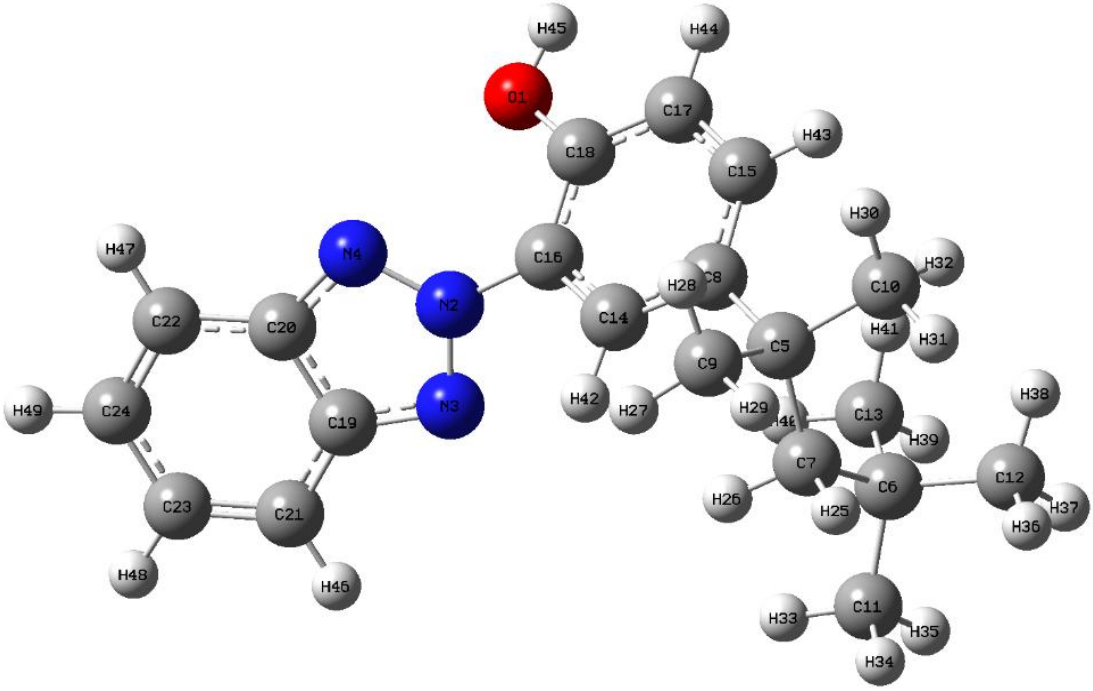

Fig. 1. Optimized structure of Octrizole.

Table 1. Optimized molecular geometry of Octrizole.

Bond length (Å)	Theoretical data	Bond angle (°)	Theoretical data
O1 -C18	1.363	C18-O1-H45	109.1
O1-H45	0.972	O1-C18-C16	121.1
N2-N3	1.340	O1-C18-C17	118.9

N2-N4	1.340	N3-N2-N4	118.8
N2-C16	1.385	N3-N2-C16	120.6
N3-C19	1.343	N2-N3-C19	102.5
N4-C20	1.343	N4-N2-C16	120.6
C5-C7	1.572	N2-N4-C20	102.5
C5-C8	1.542	N2-C16-C14	119.3
C5-C9	1.556	N2-C16-C18	120.7
C5-C10	1.543	N3-C19-C20	108.1
C6-C7	1.564	N3-C19-C21	129.7
C6-C11	1.549	N4-C20-C19	108.1
C6-C12	1.541	N4-C20-C22	129.7
C6-C13	1.533	C7-C5-C8	113.0
C7-H25	1.101	C7-C5-C9	106.9
C7-H26	1.100	C7-C5-C10	110.5
C8-C14	1.370	C5-C7-C6	122.5
C8-C15	1.370	C5-C7-H25	107.3
C9-H27	1.095	C5-C7-H26	107.6
C9-H28	1.097	C8-C5-C9	106.5
C9-H29	1.097	C8-C5-C10	113.8
C10-H30	1.098	C5-C8-C14	118.2
C10-H31	1.097	C5-C8-C15	118.1
C10-H32	1.090	C9-C5-C10	105.6
C11-H33	1.096	C5-C9-H27	113.0
C11-H34	1.096	C5-C9-H28	111.3
C11-H35	1.096	C5-C9-H29	110.8
C12-H36	1.095	C5-C10-H30	111.5
C12-H37	1.097	C5-C10-H31	110.7
C12-H38	1.093	C5-C10-H32	113.8
C13-H39	1.098	C7-C6-C11	107.1
C13-H40	1.094	C7-C6-C12	111.9
C13-H41	1.091	C7-C6-C13	114.0
C14-C16	1.395	C6-C7-H25	107.5
C14-H42	1.084	C6-C7-H26	106.3

C15-C17	1.395
C15-H43	1.082
C16-C18	1.395
C17-C18	1.395
C17-H44	1.087
C19-C20	1.407
C19-C21	1.407
C20-C22	1.407
C21-C23	1.407
C21-H46	1.083
C22-C24	1.407
C22-H47	1.083
C23-C24	1.421
C23-H48	1.089
C24-H49	1.089

C11-C6-C12	106.7
C11-C6-C13	107.6
C6-C11-H33	111.1
C6-C11-H34	111.2
C6-C11-H35	111.5
C12-C6-C13	109.2
C6-C12-H36	111.5
C6-C12-H37	111.0
C6-C12-H38	111.8
C6-C13-H39	110.4
C6-C13-H40	111.6
C6-C13-H41	112.6
H25-C7-H26	104.2
C14-C8-C15	123.7
C8-C14-C16	118.2
C8-C14-H42	120.7
C8-C15-C17	118.2
C8-C15-H43	125.0
H27-C9-H28	107.4
H27-C9-H29	106.6
H28-C9-H29	107.4
H30-C10-H31	106.5
H30-C10-H32	107.2
H31-C10-H32	106.8
H33-C11-H34	107.8
H33-C11-H35	107.5
H34-C11-H35	107.6
H36-C12-H37	107.4
H36-C12-H38	108.8
H37-C12-H38	106.6
H39-C13-H40	106.5
H39-C13-H41	105.5
H40-C13-H41	109.9

C16-C14-H42	121.2
C14-C16-C18	120.0
C17-C15-H43	116.8
C15-C17-C18	120.0
C15-C17-H44	119.2
C16-C18-C17	120.0
C18-C17-H44	120.8
C20-C19-C21	122.2
C19-C20-C22	122.2
C19-C21-C23	114.4
C19-C21-H46	123.4
C20-C22-C24	114.4
C20-C22-H47	123.4
C23-C21-H46	122.2
C21-C23-C24	123.4
C21-C23-H48	118.4
C24-C22-H47	122.3
C22-C24-C23	123.4
C22-C24-H49	118.4
C24-C23-H48	118.2
C23-C24-H49	118.2

3.2 Vibrational analysis

Vibrational spectroscopy determines the functional groups of the title compound. 2-(2-Hydroxy-5-tert-octylphenyl) benzotriazole has 49 atoms and 141 vibrational modes [24]. Theoretical peaks and experimental peaks obtained for FTIR and FTR are presented in Fig. 2(a) and Fig. 2(b), respectively. Vibrational assignments are listed in Table 2 with a scaling factor of 0.961 since the calculations were done in the gaseous state. O-H stretching is observed between 3600- 3400 cm^{-1} [25], and theoretically observed O-H peak is at 3684 cm^{-1} and experimentally observed FT IR peak is at 3641 cm^{-1}, which are within the range. 100% %PED value found for OH stretching, indicating the pure stretching. C-H stretching is in the range of 3000–3100 cm^{-1}[26]. For the title compound, C-H vibration was found within the range, and 100% CH stretching was observed at a peak of 3056 $cm^{-1,}$ indicating the pure CH stretching. CC bond

vibrations are seen between 1650 and 1400 [27], and the peak was observed at 1595 $cm^{-1,}$ which is found within the range. Experimental FT-IR and FT Raman peaks for C-C vibrations were seen at 1592 cm^{-1} and 1597 $cm^{-1,}$ respectively. Standard aromatic N-C vibrations are between 1335 and 1250 cm^{-1} [28], and for the title compound, vibrations were observed at 1318, 1311, 1274 $cm^{-1,}$ which were within the ranges. N-N stretching is seen between 1200-1000cm^{-1} [29], and the observed peaks (1190 and 1048 cm-1) for the chosen compound are in desirable range. Theoretical and Experimental results were comparable, and vibrational analysis determined the functional groups present in the chosen compound and thus confirmed the structure [30,31].

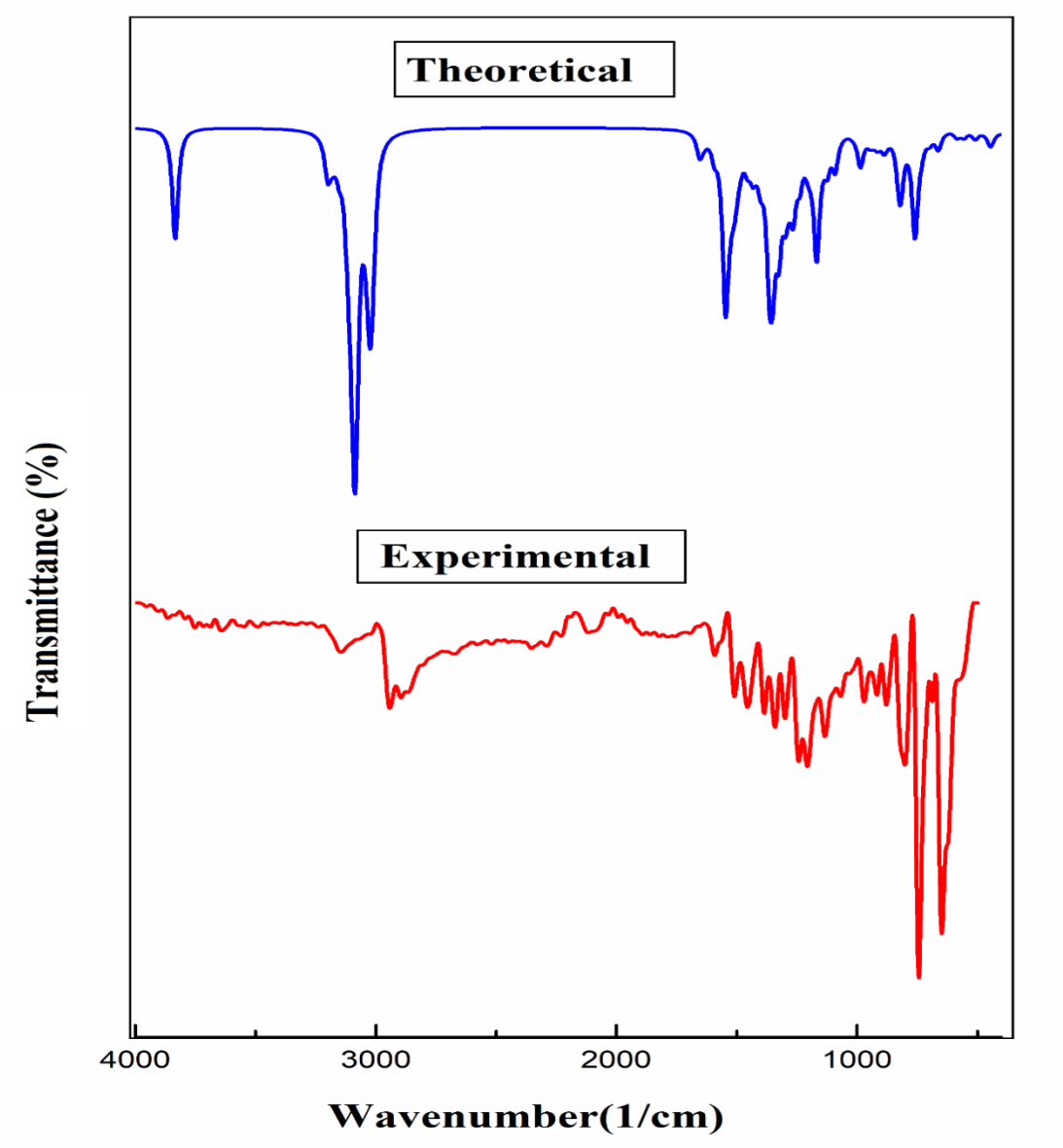

Fig. 2(a). FT-IR spectra

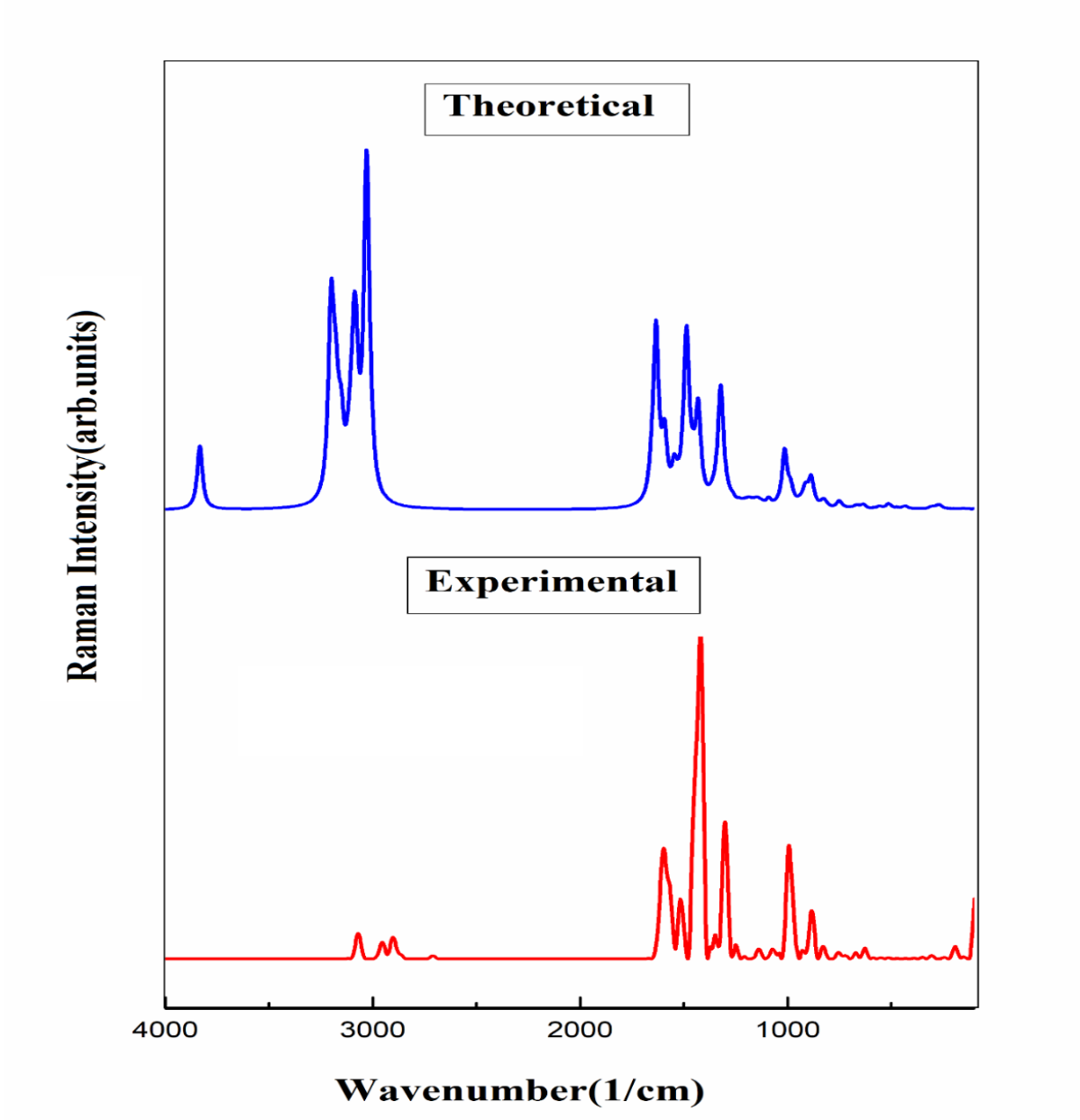

Fig.2(b) FT Raman spectra

Table 2. Experimental and calculated vibrational spectroscopic data with vibrational assignments on Octrizole.

Modes	Experimental wavenumber (cm^{-1})		Theoretical wavenumber (cm^{-1})		IR		Raman		Assignments (PED)%
	FT IR	FT Raman	Unscaled	Scaled	Rel	Abs	Rel	Abs	
141	3641		3834	3684	83	68	160	32	ϒ OH(100)
140			3207	3082	5	4	106	21	ϒ CH (93)
139			3204	3079	1	1	22	4	ϒ CH (91)

138			3200	3075	14	11	313	62	ϒ CH (91)
137		3071	3196	3072	11	9	51	10	ϒ CH(90)
136			3180	3056	9	7	192	38	ϒ CH (100)
135			3167	3044	3	3	59	12	ϒ CH(92)
134	3146		3152	3029	16	13	142	28	ϒ CH(97)
133			3120	2998	31	25	42	8	ϒ CH (87)
132			3106	2985	27	22	48	10	ϒ CH(94)
131			3104	2983	19	15	29	6	ϒ CH(97)
130			3097	2976	26	21	53	10	ϒ CH(96)
129			3090	2969	93	76	157	31	ϒ CH(52)
128			3085	2965	86	71	134	27	ϒ CH(85)
127			3085	2965	3	2	16	3	ϒ CH(83)
126			3080	2960	8	6	27	5	ϒ CH(94)
125			3078	2958	44	36	82	16	ϒ CH(84)
124	2942	2954	3072	2952	5	4	17	3	ϒ CH(98)
123			3045	2927	19	15	29	6	ϒ CH(96)
122			3032	2914	31	25	504	100	ϒ CH(78)
121			3027	2909	27	22	268	53	ϒ CH(73)
120			3022	2904	34	28	74	15	ϒ CH(86)
119		2903	3020	2903	35	29	9	2	ϒ CH(82)
118	2895		3013	2896	30	24	43	8	ϒ CH(76)
117			3005	2888	15	12	16	3	ϒ CH(82)
116	1787	1597	1660	1595	3	3	9	2	ϒ CC(50)
115	1592		1652	1588	15	12	59	12	ϒ CC(31)
114			1634	1570	4	3	422	84	ϒ CC(44)+ βCCC(21)
113			1593	1531	13	11	153	30	βCCC(20)+ βCNN (42)
112	1510	1516	1547	1487	122	100	70	14	βHCC (49)+ βCCC(10)
111			1535	1475	1	1	10	2	ϒ CC(23) + ϒ NC(29)+ βHCC(35)
110			1530	1470	15	12	3	1	βHCH(62)
109			1522	1463	12	10	4	1	βHCH(40)
108	1455		1512	1453	10	8	7	1	βHCH(43)
107			1509	1450	7	6	3	1	βHCH(43)
106			1506	1448	15	12	2	0	βHCH(40)
105			1498	1440	2	2	19	4	βHCH(41)
104			1494	1436	4	3	50	10	βHCH(46)

103			1489	1431	2	1	24	5	βHCH(66)
102			1487	1429	2	1	155	31	ϒ CC(26)
101			1486	1428	4	3	184	37	βHCH(38)
100			1484	1426	1	0	4	1	βHCH(47)
99		1420	1479	1421	1	1	1	0	βHCH(34)
98			1456	1399	16	13	48	10	ϒ CC(14)+ βHCC(10)
97	1386		1436	1380	10	8	0	0	βHCH(40)
96			1431	1376	7	6	206	41	
95			1425	1369	7	6	21	4	βHCH(56)
94		1350	1405	1350	6	5	1	0	βHCH(80)
93			1401	1346	15	12	0	0	βHCH(62)
92			1397	1343	3	2	0	0	βHCH(43)
91			1382	1328	3	2	2	0	βHCC(10) + βHCH(16)+ τ HCCC(48)
90			1371	1318	8	6	2	0	ϒ NC(16)+ βHCC(27)
89			1364	1311	45	37	4	1	ϒ CC(14)+ ϒ NC(30)
88			1362	1309	34	28	5	1	βHOC(15)+ βHCC(22)
87	1300	1302	1350	1297	64	52	12	2	βHOC(11)+ βHCC(38)
86			1325	1274	61	50	190	38	ϒ NC(26)+ βHCC(10)
85			1318	1267	2	2	117	23	βHCC(10)
84	1243		1298	1248	37	30	10	2	ϒ OC(37)
83			1284	1234	14	12	7	1	βHCC(25)
82			1267	1218	24	20	5	1	ϒ OC(10)+ τ HCCC(10)
81	1207		1263	1214	22	18	7	1	ϒ CC(10)+ τ HCCC(13)
80			1239	1190	23	19	0	0	ϒ NN(71)
79			1232	1184	3	2	8	2	ϒ CC(11)+ τHCCC(26)
78			1211	1164	5	4	6	1	ϒ CC(11)+ τHCCC(21)
77			1201	1154	13	10	5	1	ϒ CC(11)+

									βHOC(21)+ βHCC(44)
76	1133		1186	1140	5	4	12	2	βHCC(10)
75			1169	1124	17	14	1	0	βHCC(59)
74			1167	1122	69	57	8	2	βHOC(21)
73			1151	1106	3	2	10	2	ϒ CC(30)+ βHCC(62)
72			1139	1094	3	3	9	2	ϒ CC(29)+ τ HCCC(13)
71	1068		1123	1080	20	16	7	1	
70			1091	1048	24	20	18	4	ϒ NN(19)+ βCCC(22)
69			1059	1018	0	0	1	0	τHCCC(23)
68			1048	1007	0	0	2	0	τHCCC(26)
67		994	1027	987	0	0	0	0	τHCCC(36)
66	971		1014	975	1	1	139	27	βCCN(46)+ βNNN(14)
65			990	952	0	0	1	0	τHCCC(75)
64			989	950	10	9	14	3	βCCN(24)+ βNNN(10)
63			984	946	15	12	27	5	ϒ CC(22)
62			963	925	0	0	1	0	τ HCCC(97)
61			961	924	0	0	0	0	τ HCCC(38)
60	918		959	922	1	1	0	0	τ HCCC(49)+τ CCCC(13)
59			948	911	5	4	4	1	βHCC(11)+ τ HCCC(13)
58			942	905	1	1	0	0	τ HCCN(10)
57			936	899	2	2	3	1	ϒ CC(11)+ βHCC(15)+ βCCC(15)+ τ HCCN(11)
56			931	895	2	1	4	1	ϒ CC(12)+ βCCC(36)
55		884	921	885	2	1	9	2	ϒ CC(20)+ τ HCCN(13)
54	878		913	877	7	6	35	7	τ HCCN(34)
53			887	853	11	9	68	13	ϒ CC(10)+ βCCC(10)
52			872	838	3	2	5	1	ϒ CC(26)+

								τ HCCC(12)
51		858	824	0	0	0	0	τ HCCN(84)
50	801	829	797	10	8	15	3	ϒ CC(30)
49		822	790	29	24	1	0	τ HCCC(67)+ ωOCCC(15)
48		816	784	17	14	7	1	ϒ CC(24)+ βCCC(12)
47	743	777	746	1	0	0	0	τ HCCC(20)+τ CCCC(34)+ τ CNNC(27)
46		760	730	72	59	0	0	τ HCCC(84)
45		752	723	2	2	10	2	τ HCCC(14)+ ωOCCC(13)+ ωNCCC(16)
44		750	721	4	4	9	2	ϒ CC(34)
43		732	704	7	6	2	0	
42	687	699	671	6	5	2	0	ωNCNN(48)
41	648	672	646	1	1	4	1	ϒ CC(21)+ βCCC(13)
40		662	636	12	10	5	1	ϒ NN(14)+ ωNCNN(10)
39		634	609	0	0	11	2	ϒ CC(45)+ βCNN(28)
38		585	562	3	3	1	0	βCCC(13)+ βCCN(13)
37		583	560	2	2	1	0	τ HCCC(21)+τ CCCC(24)+ τ CCNC(36)
36		560	538	2	2	3	1	βCCN(10)+ βCCC(11)
35		552	531	3	3	3	1	
34		514	494	3	3	12	2	
33		504	484	4	3	2	0	βOCC(15)
32		473	454	1	1	3	1	ωCCCC(17)
31		448	431	7	6	1	0	
30		443	426	4	4	1	0	τ CCCC(33)
29		431	414	2	2	6	1	τ CCCC(22)+ τ OCCC(12)
28		422	406	0	0	0	0	τ CCCC(39)
27		395	380	1	1	1	0	βCCC(37)

26		380	366	0	0	0	0	βCCC(49)+ ωCCCC(12)
25		365	351	1	1	1	0	βCCC(11)
24		359	345	2	2	0	0	βCCC(13)+ τ HCCC(44)
23		346	333	2	2	1	0	ωCCCC(11)
22		310	298	11	9	3	1	
21		306	294	58	47	2	0	βCCC(35)
20		297	285	8	7	0	0	τ HOCC(61)
19		291	280	6	5	1	0	τ HCCC(30)+ ωCCCC(10)
18		283	272	4	3	3	1	βCCC(27)
17		278	267	2	2	2	0	
16		271	260	1	1	0	0	τ CCCC(22)+ τ CNNC(24)+ ωCCNC(36)
15		268	257	1	0	7	1	βCCC(10)+ τ HCCC(11)
14		261	250	0	0	2	0	τ HCCC(51)
13		246	237	0	0	1	0	βCCC(10)
12		231	222	0	0	1	0	τ HCCC(12)
11		222	213	0	0	1	0	
10		197	189	0	0	2	0	
9		177	171	0	0	1	0	βCCC(36)
8		153	147	1	1	2	0	βCCC(24)+ τ CCCC(11)
7		129	124	0	0	1	0	τ CCCC(64)
6	93	88	84	3	2	2	0	βNNC(22)+ τ CCCC(12)+ τ NCCC(23)
5		55	53	0	0	5	1	τ CNNC(17)+ τ CCCC(13)+ ωCCCC(14)
4		47	45	1	1	5	1	βNCC(13)+τ CCCC(11)+ ωCCCC(16)
3		39	37	0	0	0	0	τ NNCC(21)+ τ CCCC(52)
2		26	25	0	0	2	0	τ NNCC(51)+ τ CCCC(25)

1	25	24	0	0	8	2	τ NNCC(12)+ τ CCCC(53)

ϒ- stretching, β – In-plane bending, ω – Out of plane bending, τ – Torsion.

*Scaling factor 0.961 for B3LYP/6-311++G(d,p) basis set.

Rel- Relative

Abs- Absolute

Normalised to 100.

3.3 Nuclear Magnetic Resonance (NMR) Analysis

NMR spectroscopy is a technique based on shielding effect due to electron density around nucleus, which exploits the magnetic characteristics of particular atomic nuclei. Density Functional Theory (DFT) and GIAO method were used to predict and interpret ^{13}C NMR and ^{1}H NMR spectra. Electrons produce a shielding effect on ^{13}C and ^{1}H nuclei from external magnetic field. Larger electron density around the nucleus creates a greater shielding effect, which causes the atoms to be observed at lower chemical shifts and with lower ppm values known as upfield region. Higher ppm values are due to low electron density, which refers to a higher chemical shift and deshielding, which is termed as downfield region [32-35]. Chemical shifts determine the chemical environment of the molecule, and chemical shifts are presented in Table 3 and ^{13}C NMR and ^{1}H NMR spectra obtained are shown in Fig. 3(a) and Fig. 3(b), respectively. The chemical shift in ^{13}C NMR (Fig. 3(a)) spectral ranges was between 26.18 ppm and 155.11 ppm. Maximum ppm value was observed for C18 (155.11 ppm), which is bonded with an electronegative oxygen atom (O1), resulting in a low electron density, hence a deshielding effect. Standard chemical shifts for the carbon atoms attached to heteroatoms or alkyl groups were between 138- 160 ppm, and chemical shifts for the carbon atoms (C18, C8, C19, C20) were found to be 155.11 ppm, 151.12 ppm, 150.80 ppm, 150.17 ppm, respectively which is in the desired range. A chemical shift for C7, C5, C6, C9, C11, C12, C13, and C10 was found between 26 and 60 ppm, indicating that these are alkyl carbon atoms, and a lower chemical shift indicates the higher electron density around nucleus and thus a greater shielding effect. A chemical shift for C16 was found to be 135.45 ppm, which indicates that C16 belongs to arenes or methyl-substituted arenes. Normal chemical shift ranges for internal aromatic carbon atoms, namely (C14, C15, C23, C24), are between 129.5- 133 ppm, indicating a higher ppm value due to lower electron density. These results were complemented by the molecular

geometry for internal aromatic carbon atoms, which have similar bond lengths. C17, C21, and C22 have chemical shifts of 117.74, 123.4, and 124.3 ppm, respectively, where the standard range for protonated arenes is from 118-129.5 ppm [36].

^{1}H NMR spectra ranged from 0.418 ppm to 8.149 ppm. Hydrogen atoms (H 47, H46, H42, H49, H48, H43, H44) are attached to aromatic rings, showing higher chemical shifts between 6-8.5 ppm. Higher chemical shifts for hydrogen atoms in aromatic rings indicate the low electron density and a deshielding effect, suggesting the electron-withdrawing nature of aromatic rings. H45 attached to the electronegative oxygen atom has a chemical shift of 3.82, where the normative range is between 3-4 ppm, and deshielding effect observed for H45 atom was due to low electron density associated with H45, which might be suitable for biological activity. Hydrogen atoms (H32, H25, H38, H30, H27, H29, H31, H33, H34, H36, H37, H28, H35, H39, H41 and H40) present in alkyl groups shows chemical shifts of 1ppm.

Equivalent chemical shifts obtained for hydrogen atoms (H 47, H46, H42, H49, H48, H43, H44) attached to aromatic rings, suggesting that these atoms experience equivalent deshielding effects and thus are significant in determining the symmetry of chosen compound. Bond lengths of hydrogen atoms (H 47, H46, H42, H49, H48, H43, H44) attached to aromatic rings have equivalent bond lengths (Table 1), suggesting the symmetrical structure of rings and which is in line with the NMR results.

Structure determination, symmetry, and electronic interactions of the chosen compound were done by analyzing the chemical shifts obtained and comparing them with the normative chemical shifts of different functional groups [37, 38].

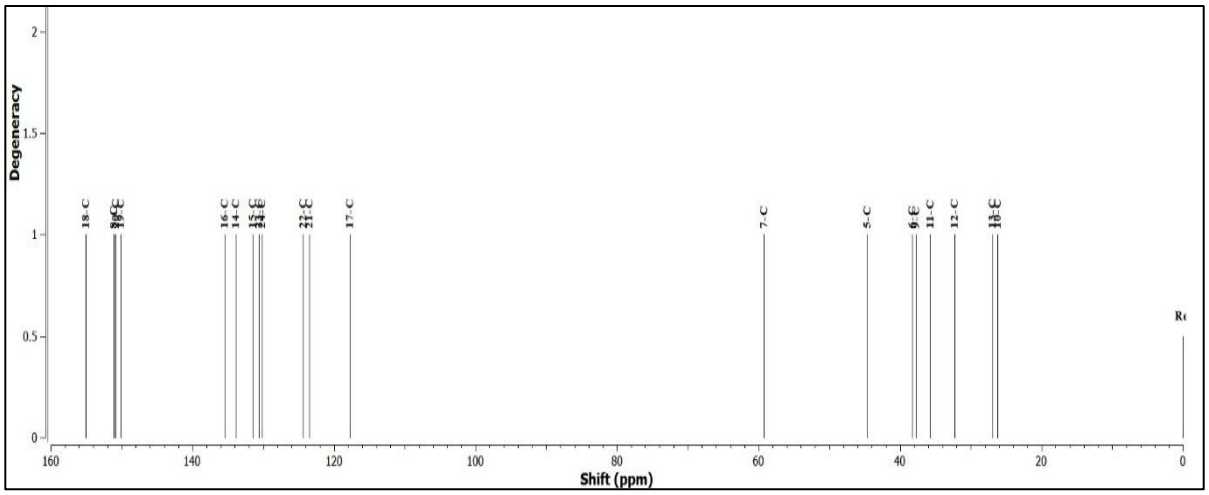

Fig. 3(a) C NMR

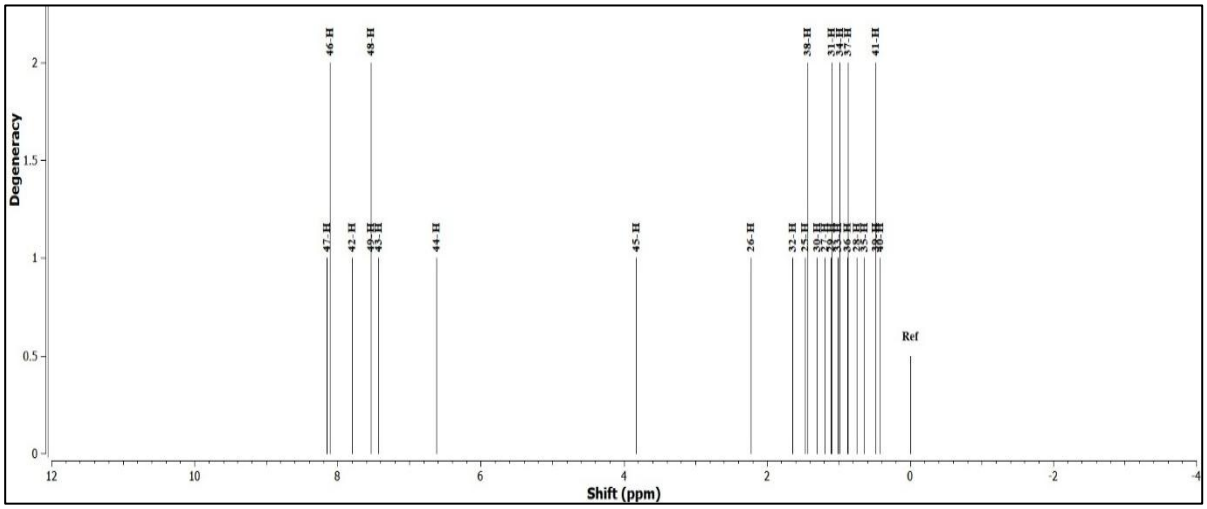

Fig. 3 (b) H NMR

Table 3 Calculated chemical shift in NMR

Atoms	Chemical shift	Atoms	Chemical shift
18-C	155.1105	47-H	8.149078
8-C	151.1276	46-H	8.103699
20-C	150.8043	42-H	7.795965
19-C	150.1777	49-H	7.536175
16-C	135.4596	48-H	7.534858
14-C	133.861	43-H	7.427326
15-C	131.4909	44-H	6.623649
23-C	130.6166	45-H	3.828516
24-C	130.1308	26-H	2.221889
22-C	124.318	32-H	1.642708
21-C	123.4456	25-H	1.465021
17-C	117.7417	38-H	1.432951
7-C	59.26357	30-H	1.298181
5-C	44.58504	27-H	1.197861
6-C	38.31644	29-H	1.106231
9-C	37.79009	31-H	1.094765
11-C	35.72784	33-H	1.011165
12-C	32.28433	34-H	0.983253
13-C	26.88927	36-H	0.877118

10-C	26.18888	37-H	0.870438
		28-H	0.748518
		35-H	0.637807
		39-H	0.483564
		41-H	0.482071
		40-H	0.418597

3.4 UV analysis

UV-Vis spectroscopy is a technique that probes the interaction between matter and electromagnetic radiation in the UV and visible spectral ranges. Electromagnetic spectrum relevant to UV-Vis spectroscopy spans from 200 nm to 800 nm, and the portion below 400 nm is designated as the UV region, while wavelengths exceeding 400 nm fall into the visible region. [39, 40]. Fig. 4 displays the theoretical UV-Vis spectrum of the title compound, and Table 4 provides the corresponding electronic properties. Maximum absorption wavelength for Octrizole was observed at 270.86 nm, a value that falls in the mid-UV region, implying that exciting an electron to a higher orbital necessitates a moderate energy, suggesting that the investigated compound has moderate stability and moderate reactivity [41].

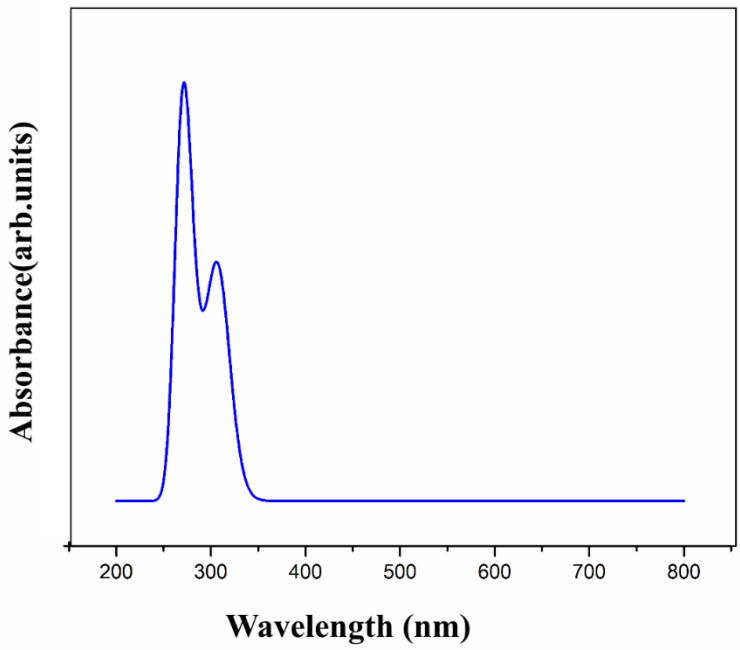

Fig. 4 UV spectra

Table 4 UV analysis

Energy (cm-1)	Wavelength(nm)	Osc.Strength	Assignments >10%
32470.49	307.97	0.1643	HOMO->LUMO (93%)
34401.39	290.68	0.0502	H-1->LUMO (93%)
36926.73	270.806	0.3133	H-2->LUMO (90%)

3.5 Frontier Molecular Orbital (FMO)

Insights into a molecule's bioactivity can be effectively gained through the analysis of its molecular orbitals, and the energy gap between the highest occupied and lowest unoccupied molecular orbitals is a fundamental predictor of its stability and reactivity. A smaller energy gap between the HOMO and LUMO predicts higher reactivity, whereas a larger gap suggests lower reactivity [42-44]. Fig.5 showcases the HOMO-LUMO energy transition, and Table 5 shows the global parameters. HOMO energy was found to be -6.359 eV and LUMO was -1.749 eV and the energy gap was 4.610 eV. Calculated wavelength using the expression $E = h\nu$ was found to be 269 nm, and thus, Frontier Molecular Orbital (FMO) studies and UV-Vis spectroscopy are consistent, both suggesting moderate stability and moderate reactivity for the molecule. An ionization potential (IP) of 6.359 eV was calculated for the compound, representing the energy needed to remove an electron. This IP value is inherently related to the HOMO energy, which corresponds to the orbital from where the electron might be removed. Calculated electron affinity (EA) of 1.749 eV for the compound represents the energy liberated when an electron is added to it. This value is directly associated with the energy of LUMO, which is the orbital that accepts electrons [45]. Title compound displays an electronegativity of 4.054, a measure of its ability to attract the electrons in a shared pair during bond formation. [45]. A Chemical Hardness (CH) value of 2.305, indicating that the chosen compound might be moderately stable, suggesting that it is a moderately hard material, and the same was predicted in UV analysis also [46]. A softness value of 0.217, which is less than 2 [47], indicates that the title compound might be less toxic. Electrophilicity index (3.565) reflects a compound's electrophilic nature, where the EI value was found to be greater than 1.5 eV, indicating the strong electrophilic nature and thus, its potential biological activity [48-50].

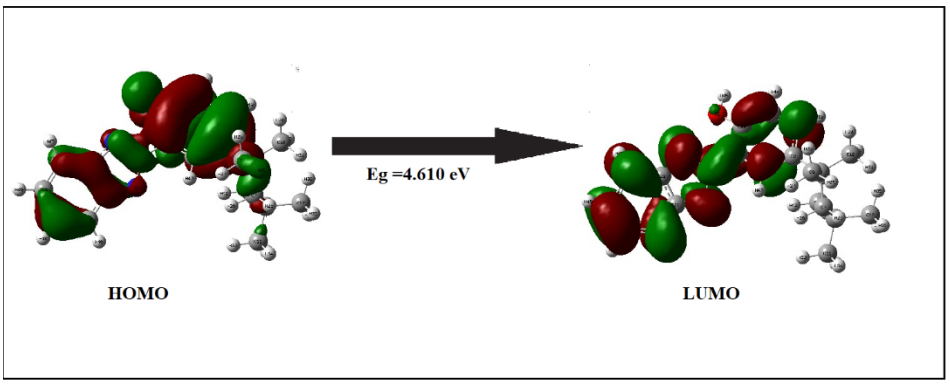

Fig. 5. Frontier molecular orbital of Octrizole.

Table 5. Calculated global parameters of Octrizole.

Parameter	Value
HOMO (eV)	-6.359
LUMO (eV)	-1.749
Ionization potential	6.359
Electron affinity	1.749
Energy gap (eV)	4.610
Electronegativity	4.054
Chemical potential	-4.054
Chemical hardness	2.305
Chemical softness	0.217
Electrophilicity index	3.565

3.6 MOLECULAR ELECTROSTATIC POTENTIAL

Molecular Electrostatic Potential creates a colored plot of Octrizole in three dimensions. MEP assesses the molecule's low and high electron densities and represents electron-donor and acceptor species. Color grading indicates that electrophilic attacking sites are found in red areas with negative potential in the map, whereas nucleophilic attacking sites are found in blue regions with positive potential and neutral electron density in green areas. Fig. 6 displays MEP map and scale starting from $-6.466e^{-2}$ to $6.466e^{-2}$ [51,52]. Blue region near H45 indicating the positive potential and therefore H45 might be a nucleophilic attacking site, which is bonded with an electronegative oxygen atom (O1), has more affinity towards electrons, making electron

cloud shift towards O1. Deshielding effect due to low electron density was observed near H45 in NMR spectra, supporting the results obtained in MEP. Nitrogen atoms (N2, N3, N4) and oxygen (O1) in the map have negative potential, which is seen in the reg region, suggesting electrophilic attacking sites. Low electron density and deshielding effect observed for C18 in ^{13}C NMR, which is bonded to O1, provided a good agreement with the MEP results. Most of the regions in a MEP map are colored green, typically indicating a neutral or near-neutral electrostatic potential, and these areas have a balanced distribution of electrons, resulting in neither a significant excess nor deficiency of electrons [53].

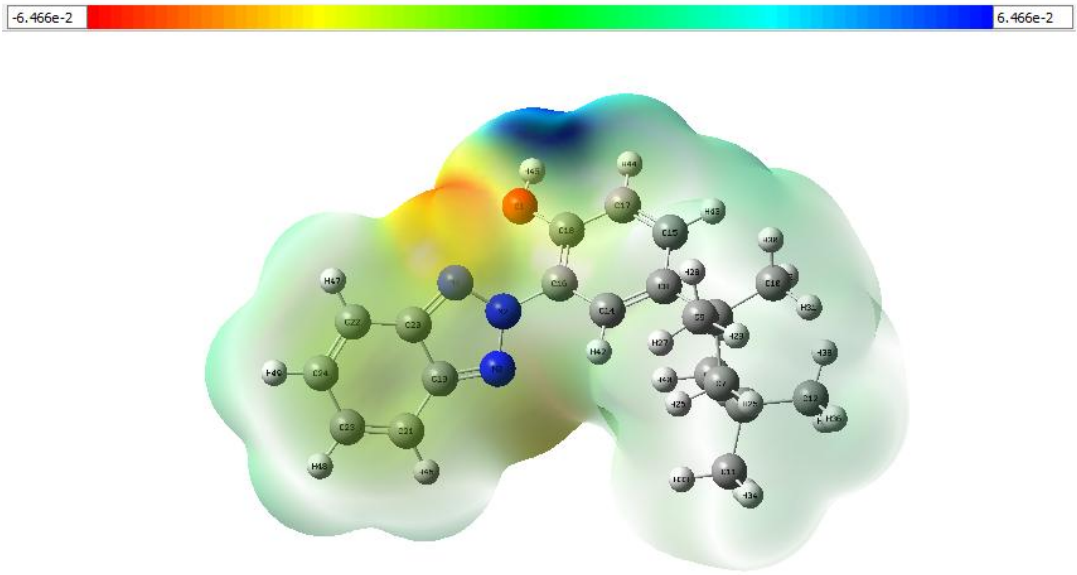

Fig. 6. Molecular electrostatic potential Map of Octrizole.

3.7 Electron Localization Function and Localized Orbital Locator

ELF & LOL are two-dimensional colored maps used in determining and approximating the electron density of the title compound [54] and are presented in Fig.7(a). and Fig.7(b).

In molecular systems, the electron distribution and Pauli's repulsion between electrons are applied to determine the Electron Localization Function (ELF) [55]. ELF scale extends from 0, represented by blue colour refers least Pauli's repulsion, to 1, represented by red colour indicates the strongest Pauli repulsion. ELF map of Octrizole displays hydrogen atoms (H34, H36) in the red area, indicating strong Paul's repulsion and maximum probability of finding an electron. Nitrogen atom (N4) and carbon atoms (C8, C14, C20, C23, C24) are in the blue area, suggesting the least Paul's repulsion.

LOL maps visualize the degree of electron depletion through color gradients [56]. LOL scale extends from 0, represented by blue colour indicating minimum electron depletion region, to 0.8, shown in red colour refers to maximum level of electron depletion. Hydrogen atoms (H34, H36) are in the red area, and Nitrogen atom (N4) and carbon atoms (C8, C14, C20, C23, C24) are in the blue area, predicting the minimum and maximum depletion, respectively. LOL offers a perspective that complements the ELF map and determines the electron distribution, Pauli's repulsion, and electron depletion within the chosen compound, which provides insight into the possible interactions for Octrizole. Low ppm value was found for H34, H36, indicating the larger electron density and greater shielding effect. ELF and LOL map of Octrizole displays that the hydrogen atoms (H34, H36) have strong Paul's repulsion and maximum probability of finding an electron near it, which is in line with NMR results [57].

.

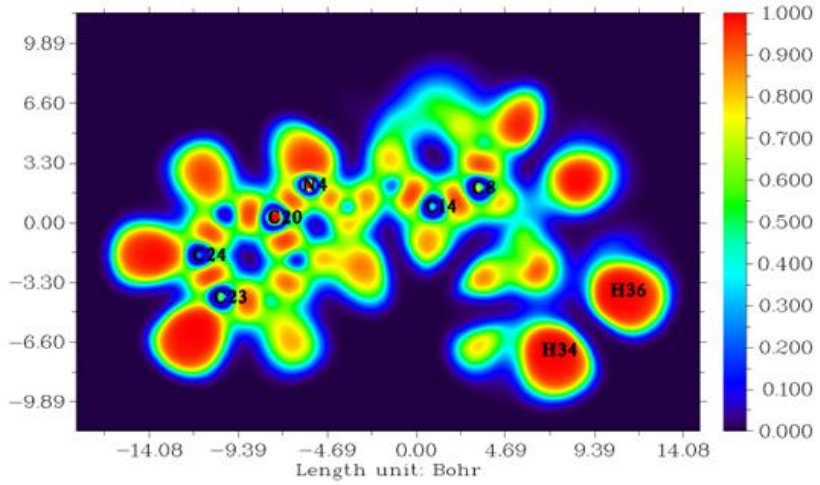

Fig. 7(a). ELF coloured map of Octrizole.

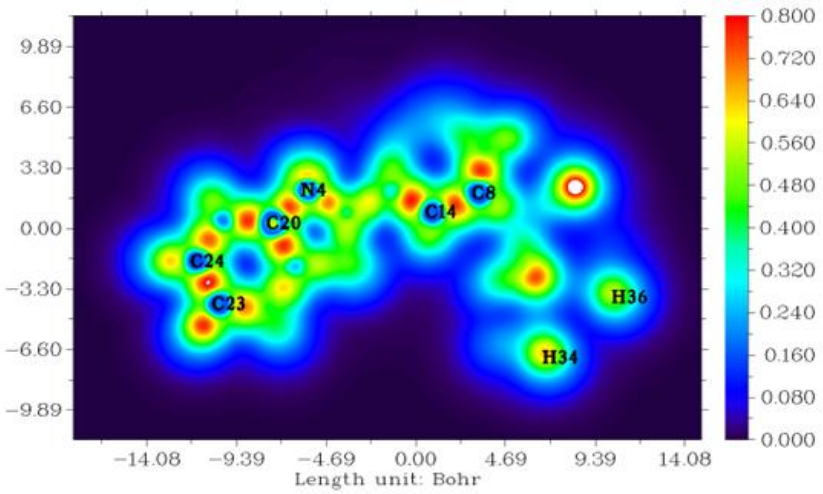

Fig. 7(b). LOL map of Octrizole

3.8 Reduced Density Gradient (RDG) Analysis

RDG is employed to calculate non-covalent interactions with the Hessian matrix and electron density [58]. Colored RDG maps can be obtained using Multiwfn 3.8 and VMD software, and Fig.8. shows the RDG map created for Octrizole, where sign(λ_2)ρ is the electron density Hessian matrix. Sign (λ_2)ρ greater than 0 and red isosurfaces indicate repulsive interactions or steric clashes, sign(λ_2)ρ less than 0 and blue isosurfaces indicate attractive interactions, and sign(λ_2)ρ near 0 and green isosurfaces are indicators of weak interactions like Van der Waals interactions. In Fig. 8, sharp peaks were seen in the red region, and red isosurfaces are observed near aromatic rings in Octrizole, suggesting the strong repulsive interactions present in aromatic rings, and the repulsion or steric clashes might be due to the closely occupied electron clouds. On comparing results from the molecular geometry of chosen compound, the longest bond lengths were observed between the carbon atoms in aromatic rings, and the results obtained in RDG are in line with each other. Green isosurface near oxygen atom indicating weak van der Waals forces near it, and it might be due to the partial negative charge on oxygen atom [59,60]. RDG plot provided information on the interactions within the molecule, which helps in understanding the biological activity of the chosen molecule.

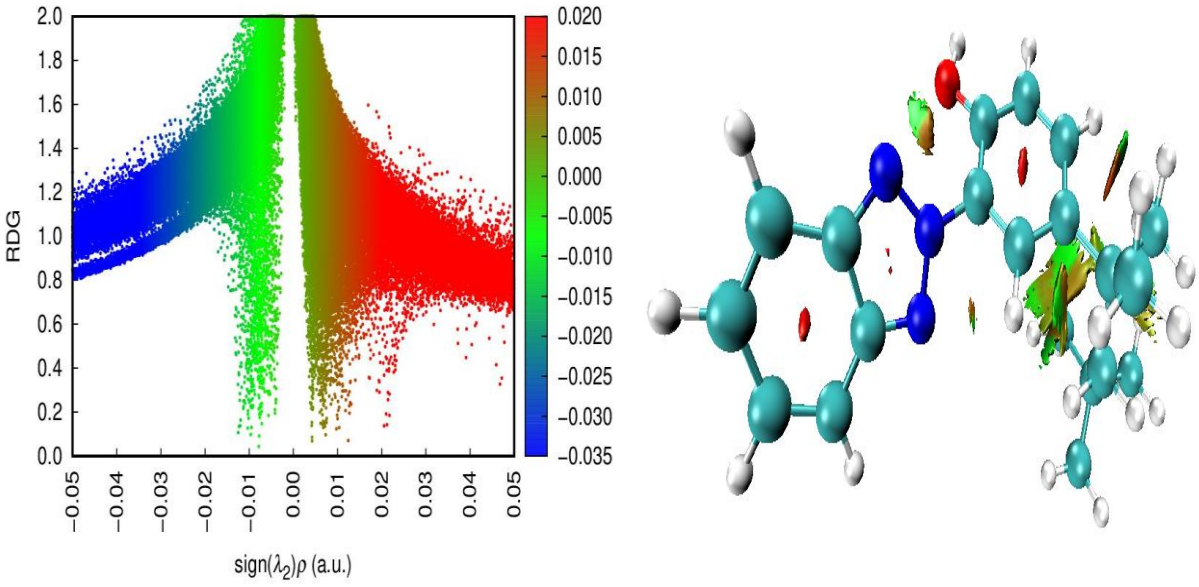

Fig. 8. RDG coloured map of Octrizole.

3.9 Mulliken Population Analysis (MPA) and Natural Population Analysis (NPA)

DFT-based Mulliken Population Analysis (MPA) is a computational approach for estimating atomic charges in a molecule and was determined by calculating the electron population associated with each atom. Atomic charges are a crucial factor in understanding molecular systems. Natural Population Analysis (NPA) gives a more accurate account of electronic charge spread throughout a molecular system, and its calculations are numerically stable. MPA and NPA were obtained using the DFT technique and are presented in Table 6. Positive charges were observed for all the hydrogen atoms present in the chosen compound, and a maximum positive charge was observed for the H45 atom in NPA (0.470). In molecular geometry, the H45 was bonded with an electronegative oxygen atom, giving rise to a partial positive charge on H45 atom. Positive potential near H45 was observed in MEP map, indicating the electron-deficient region, and the maximum positive charge observed in NPA also predicts the same. NPA analysis reveals the presence of positive charge on carbon atoms (C16, C18, C19, C20) that are attached to electronegative Oxygen (O1) and nitrogen atoms (N2, N3, N4), which might be due to the electronegativity differences between these bonding atoms. Other carbon atoms attached to hydrogen atoms showed a negative charge, where hydrogen atoms have a lower electronegativity than carbon. Oxygen atom (O1) and nitrogen atoms (N3, N4) have a negative charge, and N2 has a very low positive charge observed in NPA might be due to the higher electronegativities of O1, N2, N3, and N4. On analysing MEP map, similar trends were observed for these atoms, indicating electron-rich regions. Charges obtained for atoms in NPA were in good agreement with the results obtained in MEP analysis and which determines the possible interactions of the chosen compound [61,62].

Table 6 Mulliken and natural population of Octrizole.

Atoms	Mulliken population	Natural population
O1	-0.18938	-0.65284
N2	0.448659	0.01194
N3	-0.02334	-0.26724
N4	0.096663	-0.23877
C5	0.184084	-0.09174
C6	0.216915	-0.09289
C7	-0.34138	-0.36229

C8	0.783221	-0.03514
C9	-0.55014	-0.55594
C10	-0.35781	-0.568
C11	-0.54178	-0.56411
C12	-0.58161	-0.56814
C13	-0.5209	-0.57395
C14	-0.58924	-0.16721
C15	-0.41173	-0.18319
C16	-0.35791	0.10385
C17	-0.30581	-0.26328
C18	-0.07385	0.32369
C19	0.585641	0.09398
C20	-0.04804	0.09176
C21	-0.46211	-0.19781
C22	-0.66586	-0.194
C23	-0.17662	-0.20255
C24	-0.25133	-0.20502
H25	0.189825	0.19881
H26	0.170363	0.19943
H27	0.134197	0.20098
H28	0.166805	0.20509
H29	0.148034	0.19864
H30	0.143793	0.2011
H31	0.184611	0.20697
H32	0.118729	0.19835
H33	0.135708	0.20078
H34	0.135734	0.19718
H35	0.152314	0.19938
H36	0.145523	0.19617
H37	0.149969	0.19872
H38	0.126876	0.19742
H39	0.168311	0.19822
H40	0.212077	0.20876

H41	0.14036	0.19978
H42	0.236298	0.22519
H43	0.169733	0.21188
H44	0.159848	0.2024
H45	0.268852	0.47043
H46	0.162239	0.21597
H47	0.17584	0.21703
H48	0.17089	0.20508
H49	0.166724	0.20523

3.10 Non-linear optical activity

Non-linear optical activity arises from attractive forces of the electromagnetic fields, and Table 7 presents the NLO parameters determined by quantum chemical calculations using DFT methods. Non-linear optical (NLO) characteristic of organic molecules was elucidated by the hyperpolarizability component. Compounds that exhibit greater hyperpolarizabilities than urea fall under nonlinear optical (NLO) materials categories. Calculations are made in x, y, and z coordinates for Dipole moment, Polarizability, and First order Hyperpolarizability. Octrizole has a dipole moment (m) of 0.773D. Polarizability (α) and hyperpolarizability (β) were found to be $4.2299E^{-23}$ and $9.1484E^{-30,}$ respectively, which is more than prototype reference molecule urea ($0.452E^{-23}$ and $0.333E^{-30}$). A high polarizability and hyperpolarizability value indicate that the electron cloud can be easily distorted, which results in stronger dipoles that might contribute to Van der Waals forces (London forces), which is an interaction originating due to the dipoles. Van der Waals forces near oxygen atom were determined in RDG studies as well [63,64]. Van der Waals forces facilitate the interaction between title compound and biological systems, potentially leading to increased biological activity.

Table 7 Predicted dipole moment, polarizability, and first hyperpolarizability for basis Octrizole.

Parameters	**Value**
βxxx	679.6316276
βxxy	462.0800276
βxyy	153.9374514

βyyy	145.2489506
βzxx	128.3619
βxyz	10.6386628
βzyy	39.8919506
βxzz	-42.1649442
βyzz	69.2864657
βzzz	24.646738
βtot (a.u)	1058.933
βtot (e.s.u)	9.1484E-30
α xx	395.725147
α xy	32.8652095
α yy	263.736642
α xz	-14.0009817
α yz	24.5444005
α zz	196.78926
α (a.u)	285.4170
α (e.s.u)	4.2299E-23
Δ α (a.u)	707.4845
Δ α (e.s.u)	1.0485E-23
μx	-0.6055856
μy	-0.4671337
μz	-0.1162129
μ (D)	0.77359

3.11 Pharmacological studies

Drug likeness parameters were employed using SwissADME online software, where Lipinski's rule of Five is a guide in choosing a strong drug candidate. Table 8 presents the calculated drug likeness parameters of Octrizole and a standard drug. Hydrogen Bond Donor count was found to be 1, and Hydrogen Bond Acceptor count was 3. There are 4 rotatable bonds in the title compound, and the molecular weight was found to be 323.43g/mol. There are no infractions found for the title compound, and the parameters are within the preferred range [65,66]. High

gastrointestinal absorption indicates that the title compound is efficiently taken up from the digestive system. The blood-brain barrier (BBB) strictly regulates the passage of substances from the bloodstream into the brain. Consequently, the absence of BBB permeation indicates that the title compound is unlikely to enter the brain tissue [67]. A positive lipophilicity value of 3.46 indicates that the chosen compound might be more easily dissolvable into the lipid-based membranes than the standard drug, whose lipophilicity value was found to be -0.56, suggesting its inability to dissolve into the lipid-based membranes. Bioavailability score of 0.55 indicates good absorption and distribution into the body, like Metformin [68,69]. Drug likeness parameters obtained fall within the normative ranges and are comparable with the standard drug, Metformin, indicating the favourable drug character of 2-(2-Hydroxy-5-tert-octylphenyl) benzotriazole.

Table 8 Drug-likeness parameters for Octrizole.

Descriptor	Desirable range	Value for the title compound	Value for the standard drug(metformin)
Hydrogen Bond donors	<5	1	3
Hydrogen Bond acceptors	<10	3	2
M log P	<4.15	3.46	-0.56
GI absorption	-	high	high
Lipinski violation	-	0 violation	0 violation
skin permeation	-	-3.05cm/s	-7.99
molar refractivity	40-130	99.13	36.93
Bioavailability score	-	0.55	0.55
Number of rotatable bonds	<10	4	2
Molecular weight	<500	323.43 g/mol	129.16g/mol

8 In vitro cytotoxicity activity

In *in vitro* cytotoxicity investigation, Rat Skeletal Muscle (L6) cells were exposed to varying concentrations of 2-(2-Hydroxy-5-tert-octylphenyl) benzotriazole, ranging from 1000 to 7.8µg/mL given in Table 9. MTT assay was used to measure metabolic activity using a

colorimetric determination to examine the cytotoxic effect of specific concentrations. Number of viable cells is examined in MTT assay. Rat Skeletal Muscle (L6) cell line cytotoxicity, measured in terms of percentage cell viability, was found to be 85.39 ± 3.02% at 1000µg/mL concentration in the current investigation. An increased cell viability along with a decreased concentration is found.

Table 9. Analysis of the in vitro cytotoxicity of Octrizole against Rat Skeletal Muscle (L6) cell line by MTT assay.

Concentration (µg/mL)	Percentage of cells viable after treatment
1000	85.39±3.02
500	90.05±2.39
250	93.85±2.57
125	94.58±1.85
62.5	95.02±2.17
31.25	96.96±0.54
15.628	98.85±1.20
7.8	99.14±1.00

3.12 Ramachandran plot

Representation of Ramachandran plots served as verification of the protein stability and binding affinity. 4GQR (Human Pancreatic alpha-amylase in complex with myricetin) [70], 7KPI (Crystal structure of the SPOP MATH domain) [71], and 4W93(Human pancreatic alpha-amylase in complex with montbretin A) are proteins with properties against diabetics that were chosen for docking. Using Discovery Studio software, RC plots were obtained and shown in Fig. 9(a), 9(b), and 9(c). Allowed domain contains a majority of the protein's sequences, and a few amino acids are located in the restricted region. Stability of 4GQR and 7KPI, 4W93 was indicated by their RC plots, as a large number of amino acid residues are located inside the permitted zone, and these proteins are suitable for molecular docking [72].

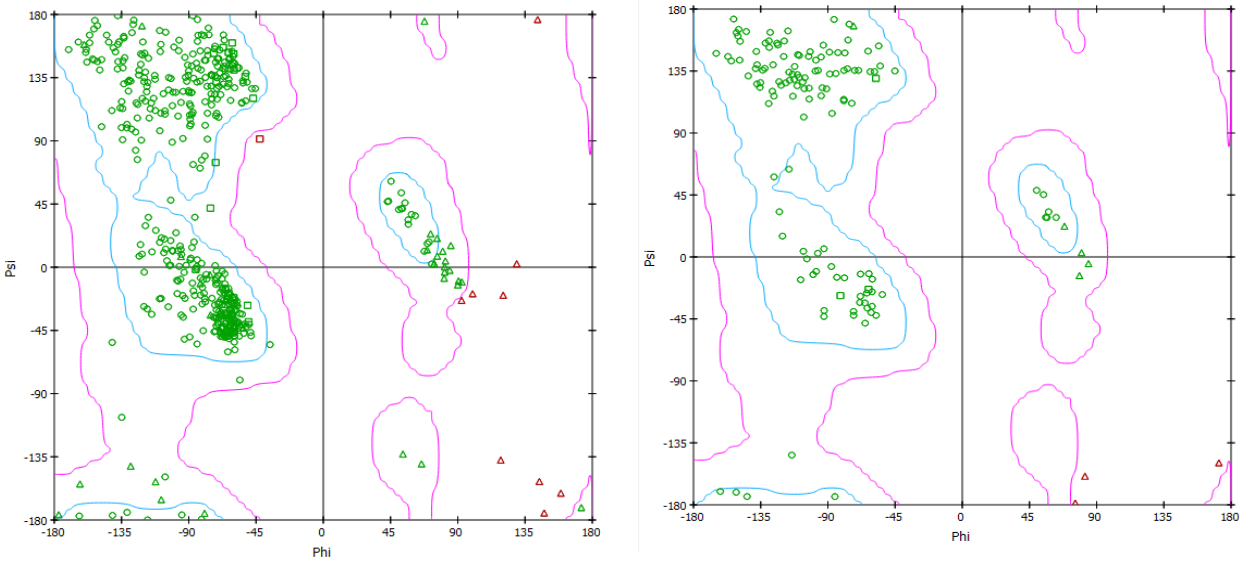

9(a) 4GQR 9(b)7KPI

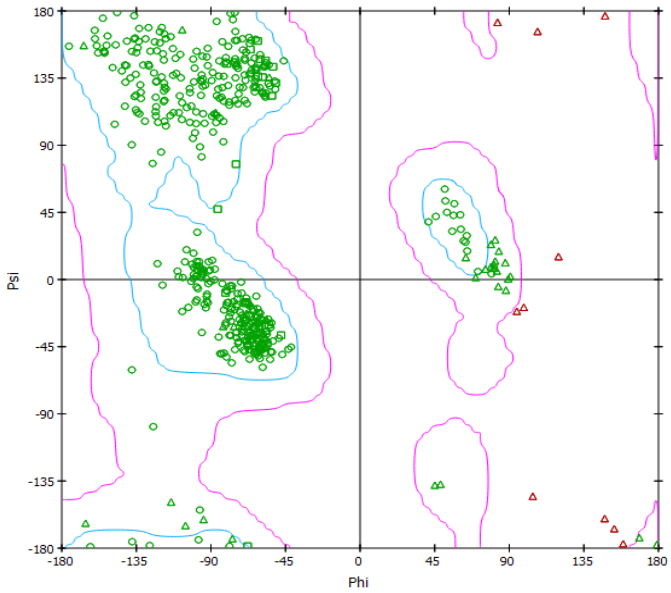

9(c) 4W93

Fig. 9. Ramachandran plots of proteins

3.13 Molecular docking studies

Docking is a widely used method for researching drugs and is an expressive technique and efficient method to explain ligand-protein interaction. Biological activity of Octrizole was assessed with PASS online program, and potency of compound under study to treat diabetics

was determined. Chosen compound was docked against 4GQR and 7KPI, 4W93 proteins using AutoDock tools 1.5.6, and visualization was done with Discovery Studio visualizer. Docking results are listed in Table 10, and ligand-protein interactions in 2 dimensions and 3 dimensions are given in Fig.10. Binding energy for 4GQR is -6.1 kcal/mol, and for 7KPI is -7.53 kcal/mol [73,74]. Title compound was also docked with protein 4W93, and binding energy was found to be -4.96 kcal/mol. Metformin is a clinical drug for diabetics and is docked against the protein Human α-amylase (4W93), which has a binding energy of -4.5 kcal/mol and is comparable with the chosen compound [75]. Compound under research has more negative binding energy than the standard drug. On comparing the bond parameters and the 2D docking diagram, ligand-protein interactions were found for the hydrogen atom (H45), where H45 was bonded to a highly electronegative oxygen (O1). A partial positive charge of H45 due to the lower electronegativity than O1, which might act as an HBD and lead to protein interaction. Other protein interactions were found for nitrogen atoms, where nitrogen atoms might be HBAs. HBD and HBA counts obtained in drug-likeness are in line with the docking results. Weak hydrogen bonds were important in ligand-protein interactions and thus the biological activity of Octrizole. Results obtained from docking and other studies suggest that Octrizole might be biologically active and has strong anti-diabetic properties.

Table 10 Molecular docking of Octrizole.

Protein (PDB ID)	**Bonded residues**	**Bonded distance(A°)**	**Binding energy (kcal/mol)**	**Reference RMSD(Å)**
4GQR	SER 108	2.083	-6.1	40.33
	SER 108	2		
	ARG 343	1.917		
7KPI	GLY 132	1.907	-7.53	22.679
	UNL 1	2.772		
	UNL 1	2.861		

4W93	UNK0 UNK0 GLN441 UNK0	2.95142 2.62761 3.14302 5.3125	-4.96	64.554
4W93(with standard	ASP 197 GLU 233	-	-4.5	-

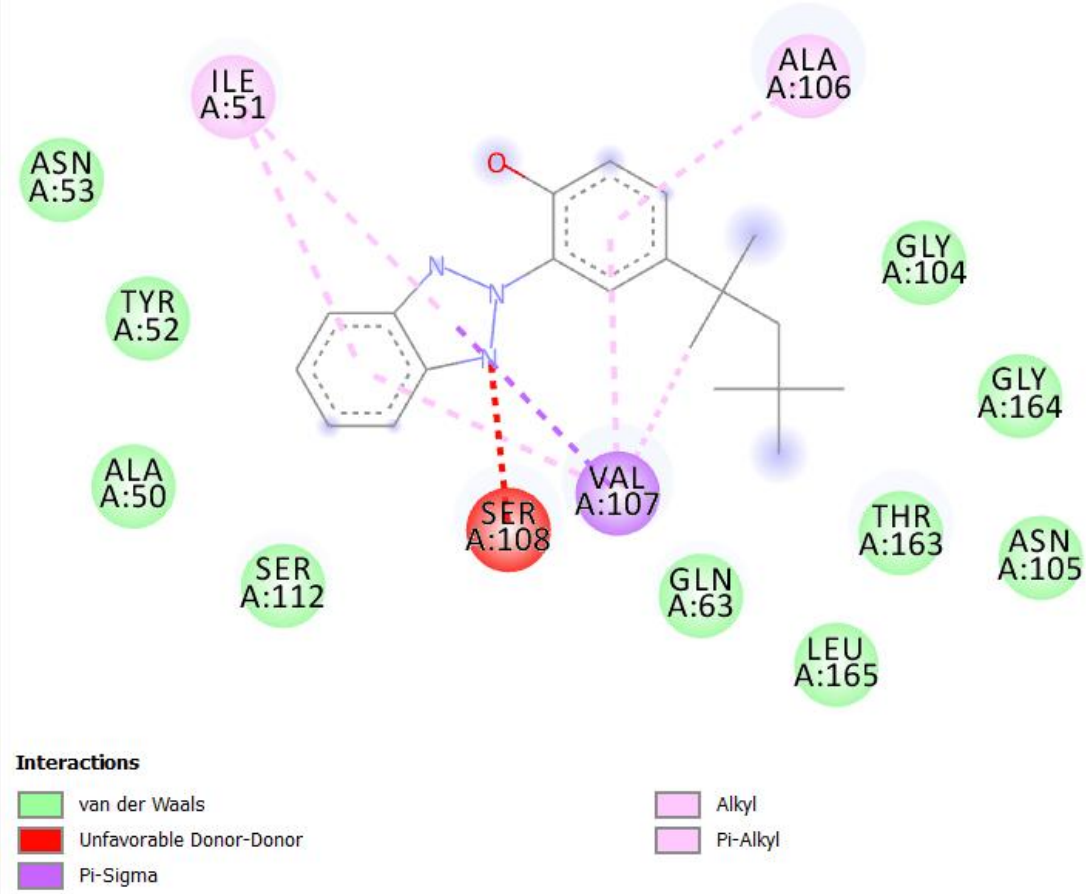

10(a)2D docking diagram of 4GQR with Octrizole.

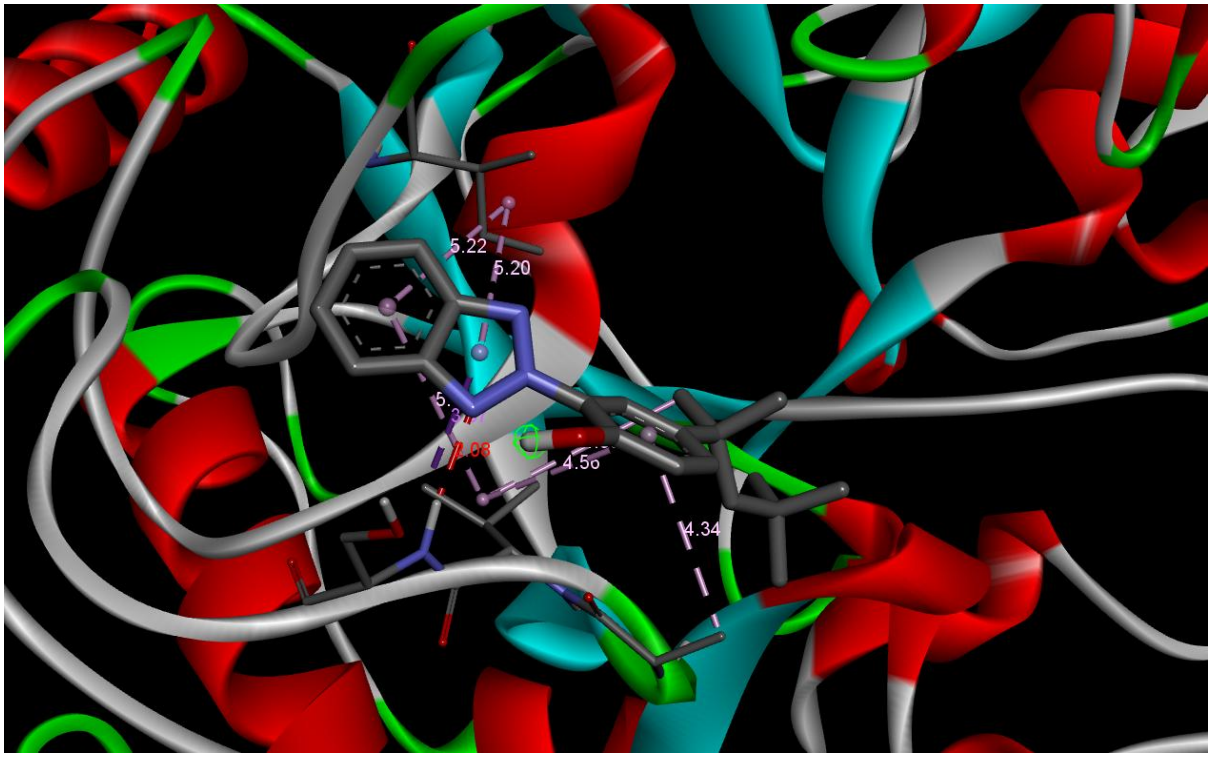

10(b) 3D docking diagram of 4GQR with Octrizole.

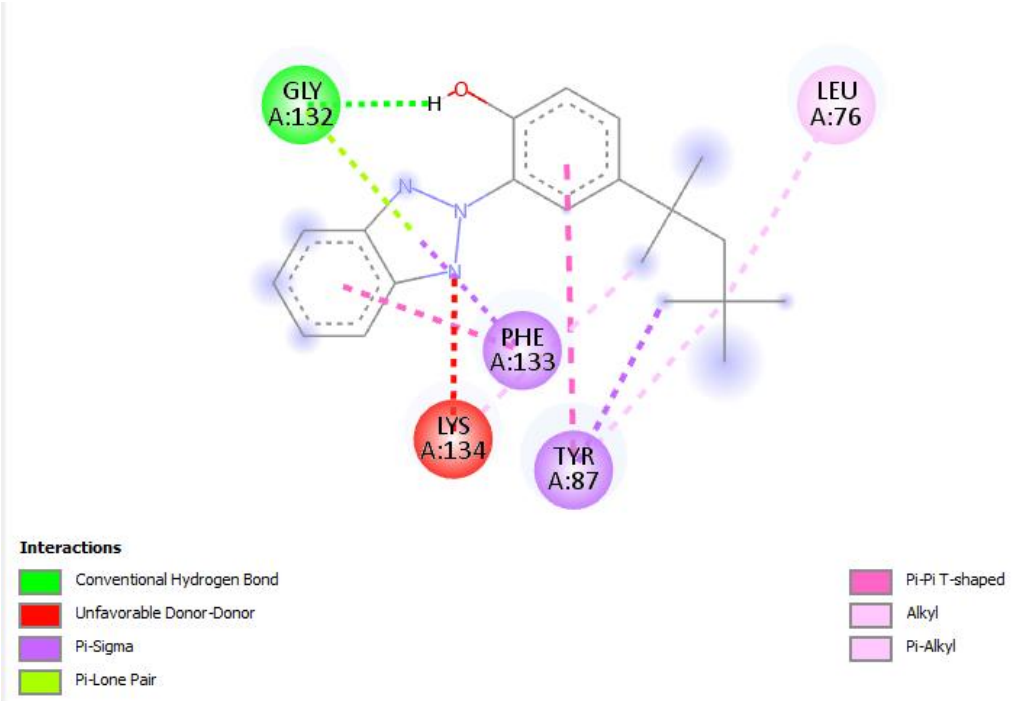

10(c)2D docking diagram of 7KPI with Octrizole.

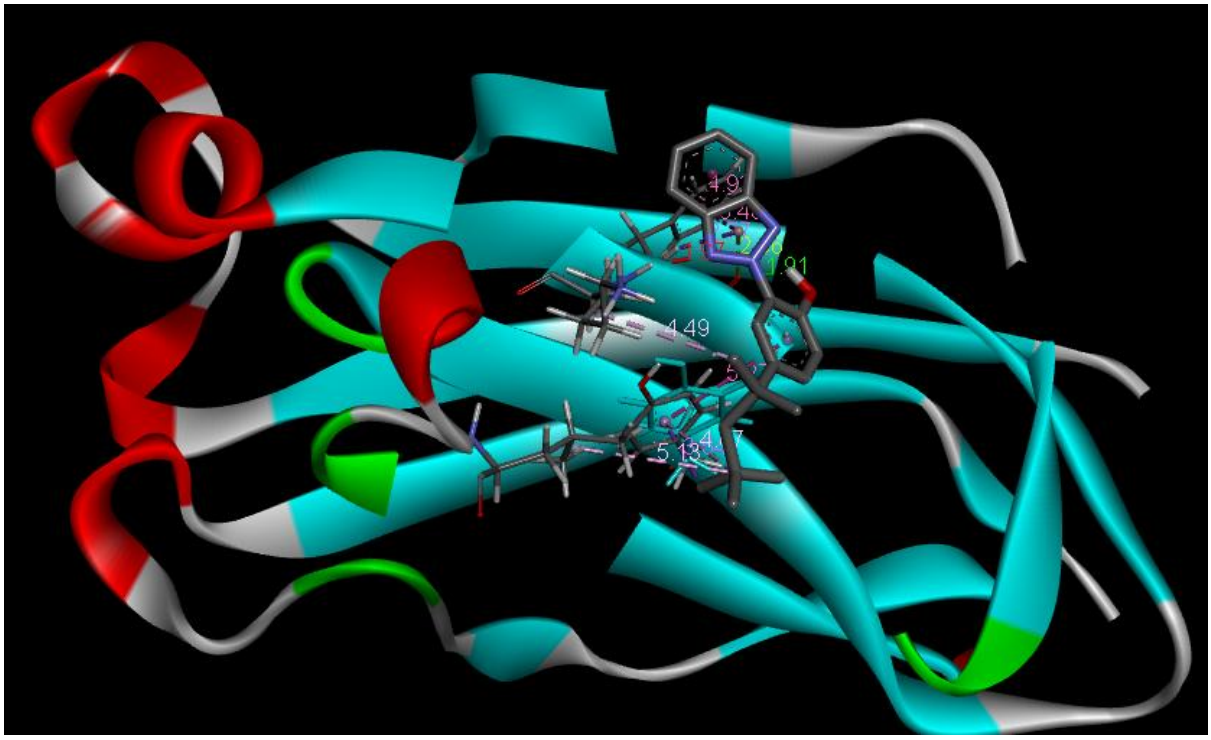

10(d) 3D molecular docking diagram of 7KPI with Octrizole

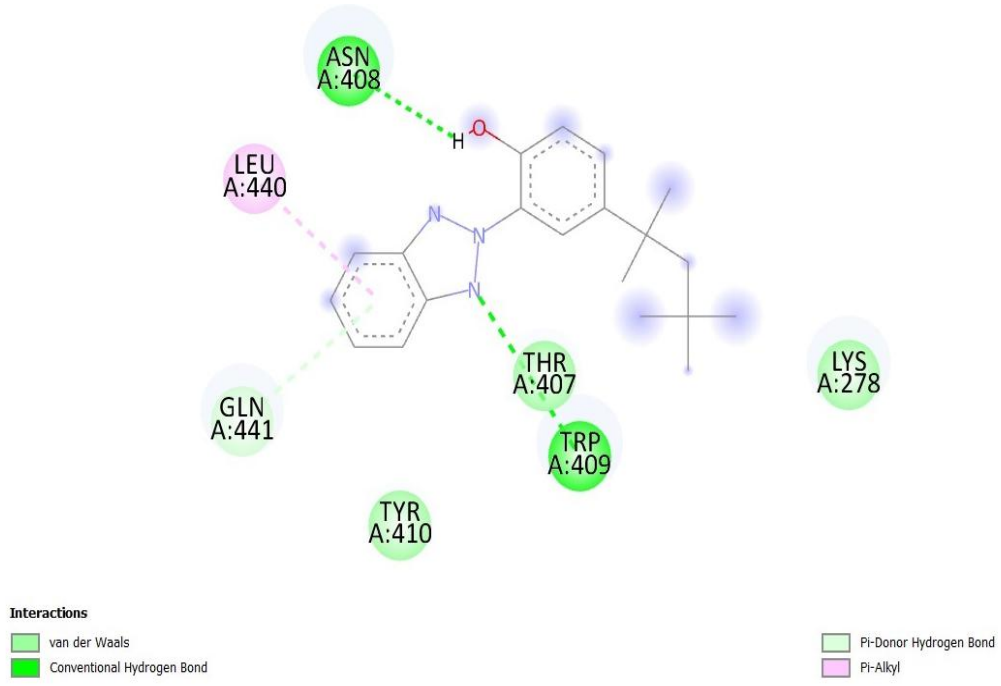

10(e) 2D docking diagram of 4W93 with Octrizole.

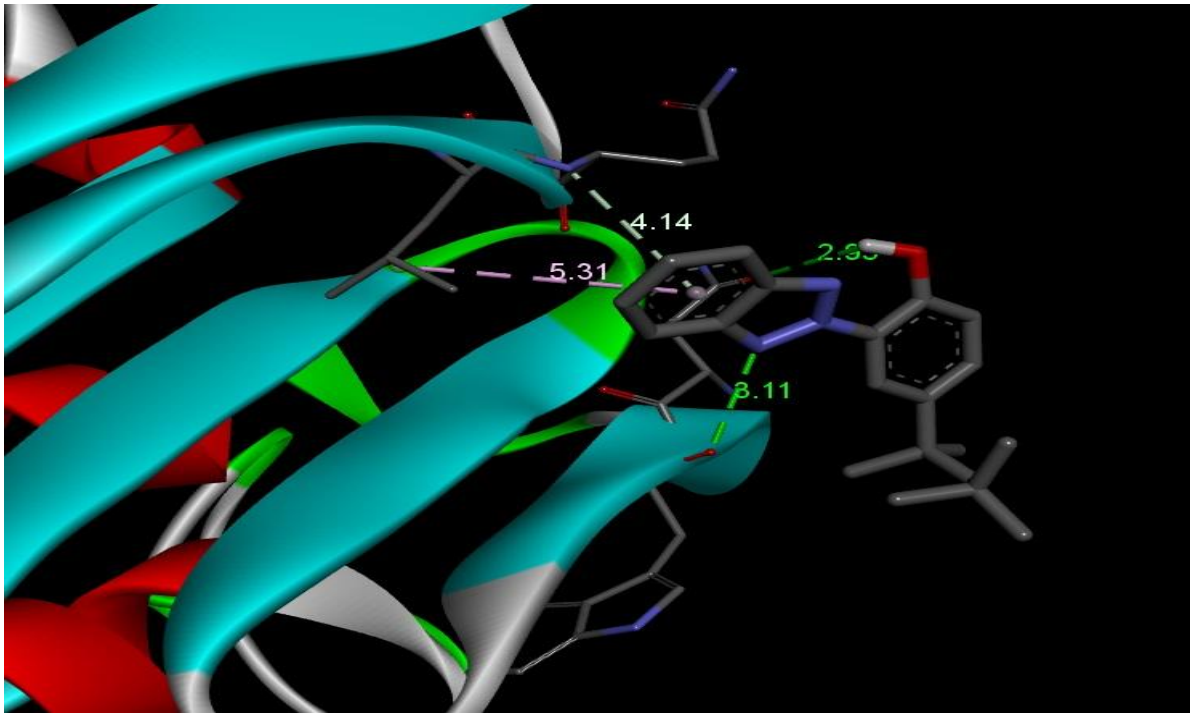

10(f) 3D molecular docking diagram of 4W93 with Octrizole

Fig.10. Molecular docking diagrams of Octrizole.

4 CONCLUSION

Density-based computational analysis with Gaussian software package and biological activity prediction on Octrizole were carried out. Optimized structure was obtained, and molecular geometry provided insights into the structure of Octrizole. Shortest Bond length (0.972Å) was found between O1 and H45. High electronegativity of oxygen that hydrogen might be responsible for the stronger attraction of hydrogen towards oxygen and thus leading to the shortening of the bond length. Vibrational analysis was employed in identifying the functional groups and thus confirmed the structure. Theoretically observed O-H peak is at 3684 cm^{-1}, which is within the range, and 100% OH stretching was found at mode 141. C-H vibration was found within the range, and 100% CH stretching was observed at mode 136 with a peak of 3056 cm^{-1}. Structure determination of the chosen compound was done by analyzing the chemical shifts obtained in NMR studies. The chemical shift in ^{13}C NMR spectral ranges was between 26.18 ppm and 155.11 ppm, and ^{1}H NMR spectra ranged from 0.418 ppm to 8.149 ppm. Carbon atoms attached to alkyl groups or attached to heteroatoms (C8, C18, C19, C20)

showed chemical shifts between 138 and 160 ppm, which is in the desired range. Hydrogen atoms (H 47, H46, H42, H49, H48, H43, H44) are attached to aromatic rings, showing chemical shifts between 7-8 ppm. Maximum absorption wavelength obtained in UV analysis was observed at 270.86 nm, a value that falls within the mid-UV region of the electromagnetic spectrum, indicating moderate stability and reactivity. HOMO energy was found to be -6.359 eV and LUMO was -1.749 eV and the energy gap was 4.610 eV. A softness value of 0.217, which is less than 2, indicates that the title might be low toxic. Electrophilicity index, 3.565 greater than 1.5 eV, indicating the strong electrophilic nature and thus, its potential biological activity. MEP map provided the possible interactions significant in determining the biological activity of Octrizole. Positive potential near the H45 atom and negative potential near Oxygen and nitrogen atoms indicated the possible reactive sites. A hyperpolarizability value greater than urea indicated that the chosen compound was NLO active and reactive. H34 and H36 in the red area indicated a maximum probability of finding an electron, and the Nitrogen atom (N4) and carbon atoms (C8, C14, C20, C23, C24) are in the blue area, suggesting the least Paul's repulsion in ELF map. LOL map also exhibits a correlation with ELF, where H34 and H36 are seen in the blue region and N4, C8, C14, C20, C23, and C24 in red region. RDG plot shows red isosurfaces near aromatic rings, indicating the repulsive interaction for aromatic rings, and the same results were identified in molecular geometry. Mulliken population analysis and Natural population analysis were carried out, and NPA shows a very good agreement with the MEP results. Maximum positive charge was observed for the H45 atom, which was bonded with an electronegative oxygen atom, and negative charges were observed for oxygen and nitrogen atoms, indicating that it might be an electron-rich species. Drug likeness parameters, namely, LRoF, GI absorption, lipophilicity, BBB, and bioavailability score, fall within the normative ranges, which were comparable with the standard drug, Metformin, indicating the favourable drug character of 2-(2-Hydroxy-5-tert-octylphenyl) benzotriazole. An increased cell viability along with a decreased concentration was found in in vitro assay studies. Stability of 4GQR and 7KPI, 4W93 was indicated by their RC plots since a large number of amino acid residues are located inside the permitted zone, and these proteins are suitable for molecular docking. Binding energy of title compound and standard drug metformin with protein 4W93 is -4.96 kcal/mol and -4.5 kcal/mol, respectively. Binding energy of chosen compound was found to be more negative than standard drug, suggesting that octrizole might be a potent compound. Biological evaluation of Octrizole predicts that it might be an agent in treating diabetics.

Disclosure of Interest

The authors report there are no competing interests to declare.

Author Contribution Statement

DONA BENNY: Validation, Visualization, Data curation, Writing- original draft

A. Anuradha: Writing- review and editing

Johanan Christian Prasana: Validation, Supervision, Software, Resources, Methodology.

References

[1] Suma, B.V., Natesh, N.N. and Madhavan, V., 2011. Benzotriazole in medicinal chemistry: An overview. *J. Chem. Pharm. Res*, *3*(6), pp.375-381.

[2] Briguglio, I., Piras, S., Corona, P., Gavini, E., Nieddu, M., Boatto, G. and Carta, A., 2015. Benzotriazole: An overview on its versatile biological behavior. *European Journal of Medicinal Chemistry*, *97*, pp.612-648.

[3] Jamkhandi, C.M. and Disouza, J.I., 2012. Benzotriazole derivatives as antimicrobial agents, pp 123-130.

[4] López-Vallejo, F., Castillo, R., Yépez-Mulia, L. and Medina-Franco, J.L., 2011. Benzotriazoles and indazoles are scaffolds with biological activity against Entamoeba histolytica. *Journal of Biomolecular Screening*, *16*(8), pp.862-868. https://doi.org/10.1177/1087057111414902

[5] Borowski, P., Deinert, J., Schalinski, S., Bretner, M., Ginalski, K., Kulikowski, T. and Shugar, D., 2003. Halogenated benzimidazoles and benzotriazoles as inhibitors of the NTPase/helicase activities of hepatitis C and related viruses. *European Journal of Biochemistry*, *270*(8), pp.1645-1653. https://doi.org/10.1046/j.1432-1033.2003.03540

[6] Beauchard, A., Jaunet, A., Murillo, L., Baldeyrou, B., Lansiaux, A., Chérouvrier, J.R., Domon, L., Picot, L., Bailly, C., Besson, T. and Thiéry, V., 2009. Synthesis and antitumoral activity of novel thiazolobenzotriazole, thiazoloindolo [3, 2-c] quinoline, and quinolinoquinoline derivatives. *European journal of medicinal chemistry*, *44*(10), pp.3858-3865. https://doi.org/10.1016/j.ejmech.2009.04.012

[7] Wan, J., Lv, P.C., Tian, N.N. and Zhu, H.L., 2010. Facile synthesis of novel benzotriazole derivatives and their antibacterial activities. Journal of chemical sciences, 122, pp.597-606.

[8] Loddo, R., Novelli, F., Sparatore, A., Tasso, B., Tonelli, M., Boido, V., Sparatore, F., Collu, G., Delogu, I., Giliberti, G. and La Colla, P., 2015. Antiviral activity of benzotriazole derivatives. 5-[4-(Benzotriazol-2-yl) phenoxy]-2, 2-dimethylpentanoic acids potently and selectively inhibit Coxsackie Virus B5. *Bioorganic & medicinal chemistry*, *23*(21), pp.7024-7034. https://doi.org/10.1016/j.bmc.2015.09.035

[9] Sanna, P., Carta, A. and Nikookar, M.E.R., 2000. Synthesis and antitubercular activity of 3-aryl substituted-2-(1H (2H) benzotriazol-1 (2)-yl) acrylonitriles. *European journal of medicinal chemistry*, *35*(5), pp.535-543. https://doi.org/10.1016/S0223-5234(00)00144-6

[10] Boido, A., Vazzana, I., Mattioli, F. and Sparatore, F., 2003. Antiinflammatory and antinociceptive activities of some benzotriazolylalkanoic acids. *Il Farmaco*, *58*(1), pp.33-44. https://doi.org/10.1016/S0014-827X(02)00003-4

[11] Bitew, M., Desalegn, T., Demissie, T.B., Belayneh, A., Endale, M. and Eswaramoorthy, R., 2021. Pharmacokinetics and drug-likeness of antidiabetic flavonoids: Molecular docking and DFT study. *Plos one*, *16*(12), p.e0260853.

[12] Vaz, J.A. and Patnaik, A., 2012. Diabetes mellitus: Exploring the challenges in the drug development process. *Perspectives in Clinical Research*, *3*(3), pp.109-112.

[13] Agarwal, P. and Gupta, R., 2016. Alpha-amylase inhibition can treat diabetes mellitus. *Res. Rev. J. Med. Health Sci*, *5*(4), pp.1-8.

[14] Frisch, M.J., Trucks, G.W., Schlegel, H.B., Scuseria, G.E., Robb, M.A., Cheeseman, J.R., Scalmani, G., Barone, V., Petersson, G.A., Nakatsuji, H. and Li, X., 2016. Gaussian16 Revision A. 03 (Wallingford, CT: Gaussian Inc.).

[15] Dennington, Roy, Todd Keith, John Millam, Semichem Inc, Shawnee Mission KS, (2009) GaussView, Version

[16] Jamróz, M.H., Vibrational Energy Distribution Analysis; VEDA 4 Program, Warsaw, Poland, 2004–2010.

[17] Lu, T. and Chen, F., 2012. Multiwfn: A multifunctional wavefunction analyzer. *Journal of computational chemistry*, *33*(5), pp.580-592.

[18] SwissADME: a free web tool to evaluate pharmacokinetics, drug-likeness, and medicinal chemistry friendliness of small molecules. Sci. Rep. (2017) 7:42717.

[19] Filimonov, D.A., Lagunin, A.A., Gloriozova, T.A., Rudik, A.V., Druzhilovskii, D.S., Pogodin, P.V. and Poroikov, V.V., 2014. Prediction of the biological activity spectra of organic compounds using the PASS online web resource. *Chemistry of Heterocyclic Compounds*, *50*, pp.444-457, https://doi.org/10.1007/s10593-014-1496-1.

[20] R. Huey, G.M. Morris, S. Forli, Using AutoDock 4 and AutoDock vina with AutoDockTools: a tutorial, The Scripps Research Institute Molecular Graphics Laboratory 10550 (92037) (2012) 1000.

[21] Dassault Systemes BIOVIA: Discovery Studio Visualizer 21.1.0.20298, 2020.

[22] Clara, T.H., Ragu, R., Jonathan, D.R. and Prasana, J.C., 2020. Structural, optical, thermal, dielectric and Z-scan study on novel (2E)-1-(4-aminophenyl)-3-(4-benzyloxyphenyl)-prop-2-en-1-one (APBPP) chalcone crystal for nonlinear optical applications. *Optical Materials*, *109*, p.110331, https://doi.org/10.1016/j.optmat.2020.110331

[23] Fathima Rizwana, B., Prasana, J.C. and Muthu, S., 2017. Spectroscopic investigation (FT-IR, FT-Raman, UV, NMR), Computational analysis (DFT method) and Molecular docking studies on 2-[(acetyloxy) methyl]-4-(2-amino-9h-purin-9-yl) butyl acetate. *Int. J. Mater. Sci*, *12*, pp.196-210.

[24] Jomaa, I., Issaoui, N., Roisnel, T. and Marouani, H., 2021. Insight into non-covalent interactions in a tetrachlorocadmate salt with promising NLO properties: experimental and computational analysis. *Journal of Molecular Structure*, *1242*, p.130730. https://doi.org/10.1016/j.molstruc.2021.130730

[25] Michalska, D., Bieńko, D.C., Abkowicz-Bieńko, A.J. and Latajka, Z., 1996. Density functional, Hartree− Fock, and MP2 studies on the vibrational spectrum of phenol. *The Journal of Physical Chemistry*, *100*(45), pp.17786-17790. https://doi.org/10.1021/jp961376v

[26] Tanak, H. and Marchewka, M.K., 2013. FT-IR, FT-Raman, and DFT computational studies of melaminium nitrate molecular–ionic crystal. *Journal of Molecular Structure*, *1034*, pp.363-373.

[27] Barnes, A.J., Majid, M.A., Stuckey, M.A., Gregory, P. and Stead, C.V., 1985. The resonance Raman spectra of Orange II and Para Red: molecular structure and vibrational

assignment. *Spectrochimica Acta Part A: Molecular Spectroscopy*, *41*(4), pp.629-635. https://doi.org/10.1016/0584-8539(85)80050-7

[28] K.T. Workman, R.A. Firth, W.K. Gichuhi, From benzonitrile to dicyanobenzenes: the effect of an additional CN group on the thermochemistry and negative ion photoelectron spectra of dicyanobenzene radical anions, J. Phys. Chem. A 127 (2023) 181–194.

[29] L. Andrews, S.R. Davis, FTIR observation of N=N stretching fundamentals in hydrogen-bonded complexes in solid argon, J. Chem. Phys. 83 (10) (1985) 4983–4989.

[30] Rastogi, V.K., Palafox, M.A., Mittal, L., Peica, N., Kiefer, W., Lang, K. and Ojha, S.P., 2007. FTIR and FT-Raman spectra and density functional computations of the vibrational spectra, molecular geometry and atomic charges of the biomolecule: 5-bromouracil. *Journal of Raman Spectroscopy: An International Journal for Original Work in all Aspects of Raman Spectroscopy, Including Higher Order Processes, and also Brillouin and Rayleigh Scattering*, *38*(10), pp.1227-1241, https://doi.org/10.1002/jrs.1725

[31] Magdaline, J.D. and Chithambarathanu, T., 2015. Vibrational spectra (FT-IR, FT-Raman), NBO and HOMO, LUMO studies of 2-thiophene carboxylic acid based on density functional method. *IOSR J. Appl. Chem*, *8*, pp.6-14.

[32] Neal, Stephen, Alex M. Nip, Haiyan Zhang, and David S. Wishart. "Rapid and accurate calculation of protein 1 H, 13 C and 15 N chemical shifts." *Journal of biomolecular NMR* 26 (2003): 215-240.

[33] Han, Beomsoo, Yifeng Liu, Simon W. Ginzinger, and David S. Wishart. "SHIFTX2: significantly improved protein chemical shift prediction." *Journal of biomolecular NMR* 50 (2011): 43-57.

[34] Pavia, Donald L., Gary M. Lampman, George S. Kriz, and J. R. Vyvyan. "Introduction to spectroscopy, 4th." *Brooks/Cole, USA* (2009): 691-695.

[35] Solomons, TW Graham, and Craig B. Fryhle. *Organic chemistry*. John Wiley & Sons, 2008.

[36] Rakhmatullin, I.Z., Efimov, S.V., Klochkov, A.V., Gnezdilov, O.I., Varfolomeev, M.A. and Klochkov, V.V., 2022. NMR chemical shifts of carbon atoms and characteristic shift ranges in the oil sample. *Petroleum Research*, *7*(2), pp.269-274.

[37] Arjunan, V., Santhanam, R., Rani, T., Rosi, H. and Mohan, S., 2013. Conformational, vibrational, NMR and DFT studies of N-methylacetanilide. *Spectrochimica Acta Part A: Molecular and Biomolecular Spectroscopy*, *104*, pp.182-196.

[38] Jebapriya, J.C., Jonathan, D.R., Kirupavathy, S.S., Ragu, R. and Prasana, J.C., 2020. Growth and characterization of a cyclohexanone based chalcone crystal 2 (E)-(4-N, N-dimethylaminobenzylidene)-5-methylcyclohexanone for nonlinear optical applications. *Optical Materials*, *107*, p.110035.

[39] Hemachandran, K., et al. "Structural activity analysis, spectroscopic investigation, biological and chemical properties interpretation on Beta Carboline using quantum computational methods." *Heliyon* 5.11 (2019).

[40] Fathima Rizwana, B., Johanan Christian Prasana, and S. Muthu. "Spectroscopic investigation (FT-IR, FT-Raman, UV, NMR), Computational analysis (DFT method) and Molecular docking studies on 2-[(acetyloxy) methyl]-4-(2-amino-9h-purin-9-yl) butyl acetate." *Int. J. Mater. Sci* 12 (2017): 196-210.

[41] jRezvan, Vahideh Hadigheh. "Molecular structure, HOMO–LUMO, and NLO studies of some quinoxaline 1, 4-dioxide derivatives: Computational (HF and DFT) analysis." *Results in Chemistry* 7 (2024): 101437.

[42] jRezvan, Vahideh Hadigheh. "Molecular structure, HOMO–LUMO, and NLO studies of some quinoxaline 1, 4-dioxide derivatives: Computational (HF and DFT) analysis." *Results in Chemistry* 7 (2024): 101437.

[43] Rastogi, V.K., Palafox, M.A., Mittal, L., Peica, N., Kiefer, W., Lang, K. and Ojha, S.P., 2007. FTIR and FT-Raman spectra and density functional computations of the vibrational spectra, molecular geometry and atomic charges of the biomolecule: 5-bromouracil. *Journal of Raman Spectroscopy: An International Journal for Original Work in all Aspects of Raman Spectroscopy, Including Higher Order Processes, and also Brillouin and Rayleigh Scattering*, *38*(10), pp.1227-1241, https://doi.org/10.1002/jrs.1725

[44] Amalanathan, M., Suresh, D.M., Joe, I.H., Jothy, V.B., Sebastian, S. and Ayyapan, S., 2016. FT-IR and FT-Raman spectral investigation and DFT computations of pharmaceutical

important molecule: ethyl 2-(4-Benzoyl-2, 5-dimethylphenoxy) acetate. *Pharm Anal Acta*, *7*(457), pp.26-28. http://dx.doi.org/10.4172/2153-2435.1000457

[45] Miar, Marzieh, et al. "Theoretical investigations on the HOMO–LUMO gap and global reactivity descriptor studies, natural bond orbital, and nucleus-independent chemical shifts analyses of 3-phenylbenzo [d] thiazole-2 (3 H)-imine and its para-substituted derivatives: Solvent and substituent effects." *Journal of Chemical Research* 45.1-2 (2021): 147-158.

[46] Pearson, Ralph G. "Chemical hardness and density functional theory." *Journal of Chemical Sciences* 117 (2005): 369-377.

[47] Manjusha, P., et al. "A computational and spectroscopic interpretation (FT-IR, FT-Raman, UV–vis and NMR) with molecular docking studies on 3-carboxy-2-hydroxy-N, N, N-trimethyl-1-propanaminium hydroxide: A pharmaceutical drug." *Chemical Data Collections* 20 (2019): 100191.

[48] Rijal, Ramesh, Manoj Sah, and Hari Prasad Lamichhane. "Molecular simulation, vibrational spectroscopy and global reactivity descriptors of pseudoephedrine molecule in different phases and states." *Heliyon* 9.3 (2023).

[49] Kumer, A., Sarker, M.N. and Paul, S., 2019. The simulating study of HOMO, LUMO, thermo physical and quantitative structure of activity relationship (QSAR) of some anticancer active ionic liquids. *Eurasian Journal of Environmental Research*, *3*(1), pp.1-10.

[50] Magdaline, J.D. and Chithambarathanu, T., 2015. Vibrational spectra (FT-IR, FT-Raman), NBO and HOMO, LUMO studies of 2-thiophene carboxylic acid based on density functional method. *IOSR J. Appl. Chem*, *8*, pp.6-14

[51] Murray, J.S. and Sen, K. eds., 1996. Molecular electrostatic potentials: concepts and applications.

[52] Murray, J.S. and Politzer, P., 2017. Molecular electrostatic potentials and noncovalent interactions. *Wiley Interdisciplinary Reviews: Computational Molecular Science*, *7*(6), p.e1326.

[53] Bakheit, A.H., Attwa, M.W., Kadi, A.A. and Alkahtani, H.M., 2023. Structural Analysis and Reactivity Insights of (E)-Bromo-4-((4-((1-(4-chlorophenyl) ethylidene) amino)-5-phenyl-4H-1, 2, 4-triazol-3-yl) thio)-5-((2-isopropylcyclohexyl) oxy) Furan-2 (5H)-one: A combined approach using single-crystal X-ray diffraction, Hirshfeld surface analysis, and conceptual density functional theory. *Crystals*, *13*(9), p.1313. https://doi.org/10.3390/cryst13091313

[54] Jacobsen, H., 2008. Localized-orbital locator (LOL) profiles of chemical bonding. *Canadian Journal of Chemistry*, *86*(7), pp.695-702. https://doi.org/10.1139/v08-052

[55] Savin, A., Nesper, R., Wengert, S. and Fässler, T.F., 1997. ELF: The electron localization function. *Angewandte Chemie International Edition in English*, *36*(17), pp.1808-1832.

[56] Clements, R.J., Womack, J.C. and Skylaris, C.K., 2019. Electron Localisation Descriptors.

[57] Selvakumari, S., Venkataraju, C., Muthu, S., Sangeetha, P. and Rajesh, R., 2023. Vibrational spectroscopic, electronic influences, reactivity analysis and molecular docking studies of 2-Fluoro-4-iodo-5-methylpyridine. *Spectroscopy Letters*, *56*(1), pp.14-27. https://doi.org/10.1080/00387010.2022.2160462

[58] Becke, A.D. and Edgecombe, K.E., 1990. A simple measure of electron localization in atomic and molecular systems. *The Journal of chemical physics*, *92*(9), pp.5397-5403, https://doi.org/10.1063/1.458517

[59] Abraham, C.S., Prasana, J.C., Muthu, S. and Raja, M., 2018. Quantum computational studies, spectroscopic (FT-IR, FT-Raman and UV–Vis) profiling, natural hybrid orbital and molecular docking analysis on 2, 4 Dibromoaniline. *Journal of Molecular Structure*, *1160*, pp.393-405, https://doi.org/10.1016/j.molstruc.2018.02.022

[60] Demirpolat, A., Akman, F. and Kazachenko, A.S., 2022. An experimental and theoretical study on essential oil of Aethionema sancakense: Characterization, molecular properties and RDG analysis. *Molecules*, *27*(18), p.6129.

[61] Ali, M., Mansha, A., Asim, S., Zahid, M., Usman, M. and Ali, N., 2018. DFT Study for the Spectroscopic and Structural Analysis of p-Dimethylaminoazobenzene. *Journal of Spectroscopy*, *2018*(1), p.9365153.

[62] Clara, T.H., Prasana, J.C., Jonathan, D.R. and Vishwanathan, V., 2022. Structural elucidation, growth and characterization of (E)-2-(4-dimethylamino) benzylidine-3, 4-dihyronapthalen-1 (2H)-one single crystal for nonlinear optical applications. *Journal of Molecular Structure*, *1261*, p.132942

[63] Islam, N. and Chimni, S.S., 2016. DFT investigation on nonlinear optical (NLO) properties of novel borazine derivatives. *Computational and Theoretical Chemistry*, *1086*, pp.58-66.

[64] Saral, A., Manikandan, A., Javed, S. and Muthu, S., 2024. Vibrational spectra, molecular level solvent interaction, stabilization, donor-acceptor energies, thermodynamic, non-covalent interaction and electronic behaviors of 6-Methoxyisoquinoline-anti tubercular agent. *Chemical Physics Impact*, *8*, p.100392. https://doi.org/10.1016/j.chphi.2023.100392

[65] Fatima, A., Khanum, G., Verma, I., Butcher, R.J., Siddiqui, N., Srivastava, S.K. and Javed, S., 2023. Synthesis, characterization, crystal structure, Hirshfeld surface, electronic Excitation, molecular Docking, and DFT studies on 2-amino thiophene derivative. *Polycyclic Aromatic Compounds*, *43*(2), pp.1644-1675. https://doi.org/10.1080/10406638.2022.2032769

[66] Lipinski, C.A., 2004. Lead-and drug-like compounds: the rule-of-five revolution. *Drug discovery today: Technologies*, *1*(4), pp.337-341. https://doi.org/10.1016/j.ddtec.2004.11.007

[67] Gawdi, Rohin, and Prabhu Emmady. "Physiology, blood brain barrier." *StatPearls* (2020).

[68] Narvekar, Mayuri, et al. "Nanocarrier for poorly water-soluble anticancer drugs—barriers of translation and solutions." *Aaps Pharmscitech* 15 (2014): 822-833.

[69] Price, G. and Patel, D.A., 2020. Drug bioavailability

[70] Williams, L.K., Brayer, G.D, Human Pancreatic alpha-amylase in complex with myricetin, https://doi.org/10.2210/pdb4gqr/pdb

[71] Usher, E.T., Boal, A.K, Crystal structure of the SPOP MATH domain, https://doi.org/10.2210/pdb7kpi/pdb

[72] Thomas, R., Mary, Y.S., Resmi, K.S., Narayana, B., Sarojini, B.K., Vijayakumar, G. and Van Alsenoy, C., 2019. Two neoteric pyrazole compounds as potential anti-cancer agents: synthesis, electronic structure, physico-chemical properties and docking analysis. *Journal of Molecular Structure*, *1181*, pp.455-466. https://doi.org/10.1016/j.molstruc.2019.01.003

[73] Kumar, M., Ahmad, S., Garima, K., Ali, A., Arora, H., Muthu, S., ... & Javed, S. (2023). Molecular Docking and Dynamic Simulations of 2-phenoxyaniline and Quantum Computational, Spectroscopic, DFT/TDDFT Investigation of Electronic States in Various Solvents. *Chemical Physics Impact*, 100307.

[74] George, J., Prasana, J. C., Muthu, S., Kuruvilla, T. K., & Saji, R. S. (2020). Evaluation of vibrational, electronic, reactivity and bioactivity of propafenone—A spectroscopic, DFT and molecular docking approach. *Chemical data collections*, *26*, 100360.

[75] Bitew, M., Desalegn, T., Demissie, T.B., Belayneh, A., Endale, M. and Eswaramoorthy, R., 2021. Pharmacokinetics and drug-likeness of antidiabetic flavonoids: Molecular docking and DFT study. *Plos one*, *16*(12), p.e0260853. https://doi.org/10.1371/journal.pone.0260853